

AD-A144 295

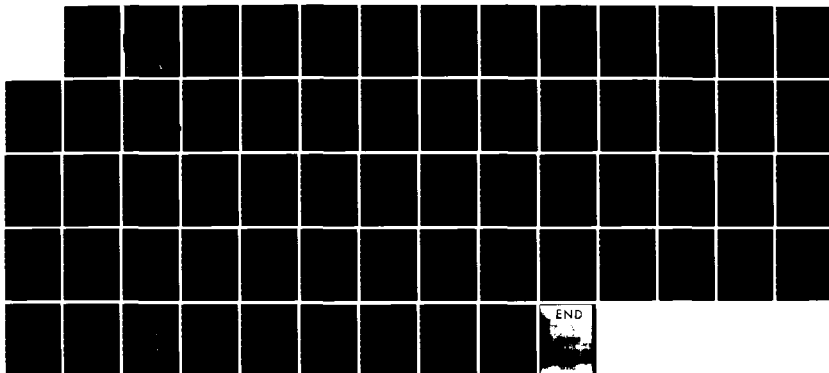
A STUDY OF POLLUTANT DISPERSAL IN A TWO DIMENSIONAL
FIELD INCLUDING GRAVITY. (U) VON KARMAN INST FOR FLUID
DYNAMICS RHODE-SAINT-GENESE (BELGIUM) S T BROWN
28 JUN 84 VKI-IN-77 EOARD-TR-84-20

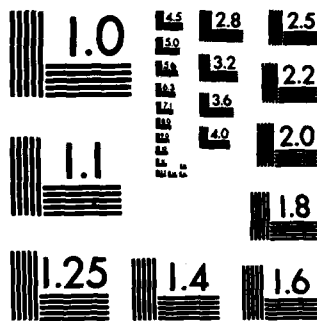
1/1

UNCLASSIFIED

F/G 20/4

NL





MICROCOPY RESOLUTION TEST CHART
NATIONAL BUREAU OF STANDARDS-1963-A

EOARD-TR-84-20

2

GRANT AFOSR 83-0146

A STUDY OF POLLUTANT DISPERSAL IN A
TWO DIMENSIONAL FIELD INCLUDING GRAVITY EFFECTS

SUSAN THOMAS BROWN
VON KARMAN INSTITUTE FOR FLUID DYNAMICS
CHAUSSÉE DE WATERLOO, 72
3 - 1640 RHODE SAINT GENÈSE, BELGIUM

JUNE 28, 1984

FINAL SCIENTIFIC REPORT, 30 APRIL 1983 - 29 APRIL 1984

APPROVED FOR PUBLIC RELEASE; DISTRIBUTION UNLIMITED

PREPARED FOR

EOARD
223,231 OLD MARYLEBONE RD
LONDON NW1 5TH
UK

DTIC
ELECTED
AUG 16 1984
S A D

84 08 07 104

AD-A144 295

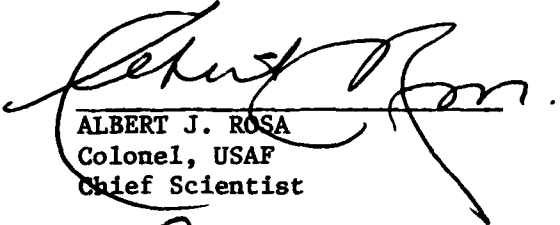
DTIC FILE COPY

REPORT DOCUMENTATION PAGE		READ INSTRUCTIONS BEFORE COMPLETING FORM	
1. REPORT NUMBER DDAD-77-84-20	2. GOVT. ACCESSION NO. H144295	3. RECIPIENT'S CATALOG NUMBER	
4. TITLE (and Subtitle) A STUDY OF POLLUTANT DISPERSAL IN A TWO DIMENSIONAL FIELD INCLUDING GRAVITY EFFECTS		5. TYPE OF REPORT & PERIOD COVERED Final Scientific Report 30 Apr 83 - 29 Apr 84	
		6. PERFORMING ORG. REPORT NUMBER VKI IN 77	
7. AUTHOR(s) S. Brown		8. CONTRACT OR GRANT NUMBER(s) AFOSR 83-0146	
9. PERFORMING ORGANIZATION NAME AND ADDRESS von Karman Institute for Fluid Dynamics Ch.de Waterloo, 72 B-1640 Rhode Saint Genèse, Belgium		10. PROGRAM ELEMENT, PROJECT, TASK AREA & WORK UNIT NUMBERS P.E. 61102F Proj/Task : 2301/D1 Work Unit No 165	
11. CONTROLLING OFFICE NAME AND ADDRESS European Office of Aerospace R&D/CA Box 14 FPO New York 09510		12. REPORT DATE June 1984	
		13. NUMBER OF PAGES 60	
14. MONITORING AGENCY NAME & ADDRESS (if different from Controlling Office)		15. SECURITY CLASS. (of this report)	
		15a. DECLASSIFICATION/DOWNGRADING SCHEDULE	
16. DISTRIBUTION STATEMENT (of this Report) Approved for public release; distribution unlimited			
17. DISTRIBUTION STATEMENT (of the abstract entered in Block 20, if different from Report)			
18. SUPPLEMENTARY NOTES			
19. KEY WORDS (Continue on reverse side if necessary and identify by block number) Density gradient Approximate factorization Pollutant dispersal Turbulent diffusivity			
20. ABSTRACT (Continue on reverse side if necessary and identify by block number) The effect of gravity forces on turbulent development is investigated both exper- imentally and numerically. In the experimental investigation, helium gas is released into an air stream. The experiment is carried out in a low speed, low turbulence wind tunnel. The He is released through an area source. Two configurations are investigated : He released from the top of the section and He released from the bottom of the sec- tion . Three different free stream turbulence levels are investigated at two free stream velocities. Numerically, the conservation of mass equation, written for a system of two spe- cies, is solved. The turbulent diffusion terms are modelled with a gradient flux model, constant coefficient of diffusivity. Comparisons are made with the experi- mental data, comparing effects of changing turbulent intensity, free stream velo- city and buoyancy. ←			

EOARD-TR-84-20

This report has been reviewed by the EOARD Information Office and is releasable to the National Technical Information Service (NTIS). At NTIS it will be releasable to the general public, including foreign nations.

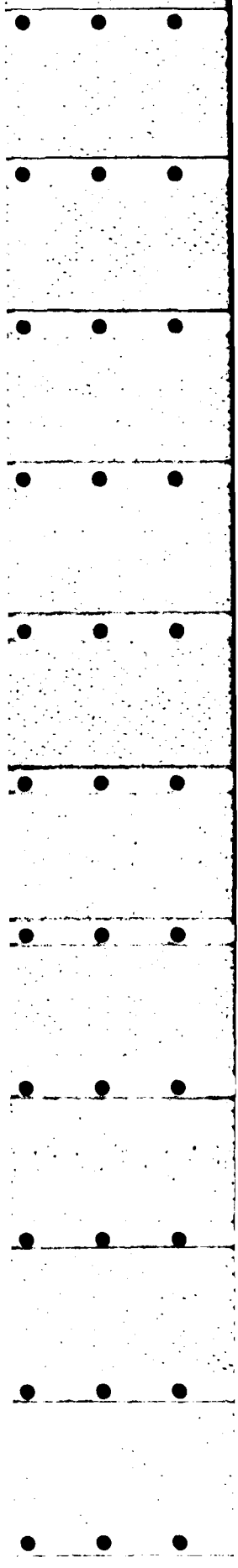
This technical report has been reviewed and is approved for publication.



ALBERT J. ROSA
Colonel, USAF
Chief Scientist



JACK O. MORRIS
Colonel, USAF
Commander



ABSTRACT

The effect of gravity forces on turbulence development is investigated both experimentally and numerically.

In the experimental investigation, helium gas is released into an air stream. The experiment is carried out in a low speed, low turbulence wind tunnel. The He is released through an area source. Two configurations are investigated : He released from the top of the section, and He released from the bottom of the section. Three different free stream turbulence levels are investigated at two free stream velocities.

Numerically, the conservation of mass equation, written for a system of two species, is solved. The turbulent diffusion terms are modelled with a gradient flux model, constant coefficient of diffusivity. Comparisons are made with the experimental data, comparing effects of changing turbulent intensity, free stream velocity and buoyancy.

LIST OF SYMBOLS

c	mass fraction of gas
f	frequency of laser light
g	stretching function in x , acceleration due to gravity
h	stretching function in y
i	current through hot wire
l	length of hot wire
r_A	chemical production
t	time
u_i	velocity vector
D_{AB}	molecular diffusivity
K	wavenumber vector, diffusivity
P	potential energy
R	resistance through hot wire
T	temperature
α	ratio of density of air to density of gas
δ	boundary layer thickness, function of concentration increment
θ	dummy variable
λ	wavelength of laser light, weight for upwinding
ρ	total mass concentration
ρ_A	mass concentration of gas

Superscripts

'	fluctuating quantities, derivative
-	mean quantities, transformed coordinate system

1. INTRODUCTION

The study of the dispersal of pollutants is of major concern to all factions of society : governments, industries, communities, and to each individual personally. With the expanded use of petroleum products, including LPG and large chemical production plants, interest has recently been escalated regarding the probable outcome of large accidents with heavy gases. In the past, very approximate methods, usually loaded with empiricism, were used to predict the average concentration field of a pollutant. This is satisfactory if it is applied to mildly-toxic or non flammable emissions, and usually very large safety factors are applied to cover the weaknesses in the schemes. But in this day and age, where large amounts of highly toxic and flammable gases are being stored and transported, more accurate prediction methods are needed. To try to meet this need, many new models have been proposed, based on the physics of the problem. That is, an attempt to solve the governing equations of the flow is made. Since turbulence on all scales is present in the flow field, assumptions and simplifications must be made to make these equations soluble. Thus, the results of such studies are no more accurate than the empirical models. The models also vary in the results, one to the other, as in each, the simplifications are made in different ways and in varying degrees. A major problem with these studies is the scarcity of good experimental data, especially for the dispersion of heavy gases.

An extensive review of models and methods used in pollutant dispersal for non-buoyant gases can be found in Slade (Ref. 1). For a review of models as particularly applied to heavy gases, reference can be made to the paper by Raj (Ref. 2).

In the present study, a simple flow field is studied experimentally to provide data to increase the understanding of the phenomena of heavy gas dispersal. These data are then compared to a simple numerical scheme, using a constant coefficient

of turbulent diffusivity, with the purpose of determining the validity of such a model.

The experimental investigation consists of the release of He gas from an area source in a wind tunnel. Both negatively and positively buoyant gas releases are studied by releasing the gas from either the top of the section or the bottom of the section. Two average flow velocities at three turbulent intensities are studied. The release is such that the flow field can be considered two dimensional.

The numerical study consists of the solution of the diffusion equation by approximate factorization after the manner of Beam and Warming (Ref. 3). The velocity is assumed to be unaffected by the gas, eliminating the need to solve the momentum equation. As indicated in the previous paragraph, the field is considered two dimensional. Diffusion is non-negligible in both spatial directions, but convection in the vertical direction (perpendicular to the direction of the flow) is neglected.

2. THEORY

In the case of the dispersal of a pollutant into the atmosphere, one must consider a flow field with two gaseous species. The equation describing the diffusion of one species into another can be written (Ref. 4, p 557) :

$$\frac{\partial \rho_A}{\partial t} + \vec{v} \cdot \rho_A \vec{V} = \vec{v} \cdot \rho D_{AB} \vec{v}_C + r_A \quad (2.1)$$

where

r_A = chemical production

ρ_A = mass concentration of gas

ρ = total mass concentration

c = mass fraction of gas

D_{AB} = molecular diffusivity of gas into air.

In the case under study, there are no chemical reactions, so $r_A = 0$. ρ_A , the mass concentration, can be expressed as $c\rho_g$, where ρ_g is the density of the gas and c is the mass fraction of gas. If ρ_a is the density of air, $\rho = c(\rho_g - \rho_a) + \rho_a$. Then equation (2.1) can be written as :

$$\rho_g \frac{\partial c}{\partial t} + \rho_g \frac{\partial}{\partial x_i} c u_i = \frac{\partial}{\partial x_i} \left[\left[c(\rho_g - \rho_a) + \rho_a \right] D_{AB} \frac{\partial c}{\partial x_i} \right] \quad (2.2)$$

(Note that the usual summation convention is inferred by repeated indices).

If it is further assumed that :

$$u_i = \bar{u}_i + u_i'$$

$$c = \bar{c} + c'$$

$$\rho \sim \gamma(\rho_g - \rho_a) + \rho_a$$

$$\rho_a / \rho_g = \alpha$$

and equation (2.2) is averaged in time, we obtain :

$$\frac{\partial \bar{c}}{\partial t} + \frac{\partial}{\partial x_i} \bar{c} \bar{u}_i + \frac{\partial}{\partial x_i} \overline{c' u_i'} = (1-\alpha) \frac{\partial}{\partial x_i} D_{AB} \frac{\partial \bar{c}}{\partial x_i} \quad (2.3)$$

Equation (2.3) can be solved for the composition of the mixture if the velocity field and the turbulent dispersion terms are known. Normally, the equation of motion is solved for the velocity field and the turbulent dispersion terms are modelled in some way. In this work, it is assumed that the velocity is not changed by the presence of the gas, so it can be a known input to equation (2.3), and it is not necessary to solve the equation of motion. This simplifies the problem immensely, as then it is necessary only to solve one equation, with a model for the turbulent dispersion terms.

3. EXPERIMENTAL INVESTIGATION

3.1 Experimental method

3.1.1 Velocity measurements

A complete explanation of the LDV techniques and associated bibliography can be found in reference 5. Here the basic principles of this measurement technique and the motivation of its employment in turbulent measurements will be briefly recalled.

The laser doppler method is based on the detection of the doppler frequency of laser light scattered from small solid or liquid particles moving with the main flow.

The relation between the velocity of the particles illuminated by the laser beam, of frequency f and wavelength λ , and the doppler frequency f_D of the scattered light is linear. That is,

$$f_i - f_s = U/\lambda(K_s - K_i) \quad (3.1)$$

where

f = frequency

K = wave number vector

U = velocity vector

subscript i = incident light

subscript s = scattered light

With the LDV it is also possible to measure simultaneously two velocity components in a turbulent flow. In fact, if two pairs of orthogonal laser light beams are focused on the same point, a spatial system of internally orthogonal interference fringes is formed. If one pair of beams is shifted in frequency, for example by passage through a light frequency

shift unit such as a Bragg cell, the probe volume is composed of the superposition of a stationary fringe system and a moving one, which has a fringe velocity proportional to the frequency difference of the two shifted beams. A particle passing through this volume scatters light of two different frequencies corresponding to the components of the particle velocity with respect to fringe planes. Therefore, it is possible to separate the frequency corresponding to each velocity component by filtering the signal with two different filters. The necessary conditions to achieve this result are :

1. no overlapping in the frequencies produced by the two fringe systems, and
2. a detectable frequency difference.

From these considerations it is clear that a twin LDV with Bragg cell in one arm is a very suitable system for two dimensional velocity measurements in a turbulent flow because of its non-intrusivity, which is a very stringent requirement for the measurements of turbulent quantities, and because the two measurements can be taken simultaneously.

3.1.2 Concentration measurements

Helium concentration is measured with a probe of the kind introduced and tested by Olivari & Colin (Ref. 6). The working principle is the following. If a metallic wire, heated by an electrical current, is placed in a flow, the voltage difference between its extremes is sensitive to the variation of velocity and heat transfer properties of the flow itself, and thus to its composition, if the medium is a mixture of two gases. Therefore, in principle, it is sufficient to separate these independent variables to measure the variation of one of them, e.g. in order to determine the concentration, one can avoid the velocity dependence by placing the wire in a region of uniform velocity. To create the uniform velocity region, the probe has a constant section followed by an expansion. The wire is

placed in the center of the expansion region, where the flow behaves like the potential core of a jet. The mass flow in the probe is controlled by a sonic hole driven by a vacuum pump. In such a manner the mass flow is a function only of the concentration (and eventually temperature) variation since this parameter affects the speed of sound.

If the hot wire is placed in a region of relatively high velocity, which minimizes its sensitivity to Re variation, the simplified equation for the hot wire heat transfer is :

$$i^2 R/A = lk(T_w - T_{mix}) = A l \lambda \Delta t \quad (3.2)$$

and if the hot wire is inserted in a resistance bridge, the voltage across the bridge is :

$$v = R_B(i+i') \sim R_B i \quad (3.3)$$

Thus

$$v = R_B (L \lambda A \Delta T / R)^{1/2} \quad (3.4)$$

From this relation it is evident that there exists a dependence of the voltage wire output on both thermal conductivity and temperature, so it is again necessary to carry out a variable separation, that is, running at a constant flow temperature. Also evident is the advantage of the employment of a hot wire with very low electrical resistance in order to increase the sensitivity.

3.2 Test facilities and instrumentation

The measurements are carried out in a low speed wind tunnel (VKI L-3) whose features are : blower-driven, open-return circuit, 25/1 convergence contraction ratio, temperature

controlled, free stream turbulence level of 0.1%, cross section of 200 mm × 200 mm and a test section 2 m long.

A new test section was designed in order to generate a uniform horizontal flow with turbulence level varying in the range 2-10% and a density stratification in the vertical direction.

3.2.1 Flow system

3.2.1.1 Turbulence production

The different levels of turbulence are obtained by placing different kinds of turbulence generators and manipulators near the entrance of the test section. The choice of these turbulence manipulators is based upon the results and information contained in the work reported in reference 7, dealing with the interaction of free stream turbulence with screens and grids.

Table 3.1 specifies the manipulators selected, three different screens and one perforated plate, and summarizes some of their relevant characteristics. The table also gives the pressure drop coefficient k , the mesh Reynolds number, Re_m and the Reynolds number, Re_d , based on the wire diameter of the screens, for a free stream velocity of 3 m/s.

The solidity, σ , is always less than 45% to avoid the emergence of large scale instability associated with high solidity devices. The Re_d is always more than 30, which is the critical range in which small changes in U or upstream disturbances result in large changes in the character of the flow downstream of the manipulators.

For the final six flow conditions, the manipulators were chosen to have turbulence intensities of 16% (manipulator 1), 8% (manipulator 2) and 3% (manipulator 3).

3.2.1.2 Density gradient generation

The density gradient in the vertical direction is obtained by injecting helium through a porous wall section. The test section can be adapted such that the porous wall is on the top or on the bottom side. When He is released from the top wall, a stable stratification results, as all the energy generated by shear is used in working against the buoyancy forces, which therefore produce a loss of turbulence energy in addition to viscous dissipation. When He is released from the bottom wall, however, an unstable stratification results, as buoyancy forces transfer energy to the turbulence at a rate that is independent of height, while transfer from the mean flow is proportional to the velocity gradient and buoyancy becomes relatively larger; the ratio of turbulent intensity to shear stress increases and the eddy diffusivity is larger than that in a constant density flow.

The helium is injected through the porous section with a volume flow of 4740 ℓ/h .

The porous wall is made of plastic foam that allows the gas to perspire with an exit velocity practically equal to the filter velocity, 1.9 cm/s. As the ratio between the filter velocity and the air velocity is of the order of 1/150 or 1/300 ($u = 3$ m/s and 6 m/s, respectively), it is possible to neglect the perturbation due to the lateral injection of flow. The reference system is therefore taken as the main air flow entering the test section.

3.2.2 Experimental apparatus

3.2.2.1 Velocity measurements

A Spectra-Physics model 12A helium-neon laser source delivering a power of 15 mW is employed. After a first polarization the laser beam enters the transmitting part of the

optical system, which is composed of the following elements : triple-beam-splitter module, which splits the beam into three separate beams, two beams of equal intensity at a distance of 50 mm apart and a central beam; a second polarizer for the central beam; dual-beam splitter that splits the central beam into two equal intensity beams with a separation of 20 mm; the double Bragg cell used to shift the frequency of one of the two pairs of beams; the steering module to center the shifted beams in the plane orthogonal to the non shifted ones; and, last, a focusing lens with focal length of 333 mm.

The receiving optics consist of a photomultiplier tube RCA-97326 focused by a zoom objective. The signal from the photomultiplier is then band-pass filtered in two D0-781-3 VKI filters in order to discriminate the two velocity components (Ref. 8). Afterwards the signals enter two VKI-D0-78-31 counter data processors which give fluctuating voltage outputs directly proportional to the velocity components.

The most important parameters defining this optical system are reviewed in table 3.2 : probe volume dimensions; number of fringes inside it; fringes spacing; and pinhole diameter. In figure 3.1 a schematic view of the source with the electronics is shown.

3.2.2.2 Concentration measurements

For concentration measurements the techniques described in section 3.1.2 are adopted. The miniaturized gas concentration probe is placed in the flow field. A mechanical device, fixed on the external part of the test section wall, supports it and allows its displacement in the vertical direction (orthogonal to the flow). The output of the probe is fed to the VKI series 85 hot wire anemometer and then to an oscilloscope to visualize the signal.

This probe is not an absolute concentration sensor and as such it needs a previous calibration for the gas employed in the experiment. Moreover, since it is very sensitive to the ambient temperature the calibration is repeated each day just before starting the measurements. The sensitivity near the origin is 0.15% He in air in volume per millivolt. The response time is of the order of 1 m/s. Figure 3.2 is a schematic of the equipment employed.

3.2.2.3 System of data acquisition and reduction

Concentration and velocity profiles are taken in several sections along and downstream of the surface gas source. The main quantities to be obtained in order to understand the behavior of the concentration and velocity fields are the mean velocity and concentration, the RMS for the two velocity components and the concentration, and their respective spectra. To obtain all of that it is necessary to collect and store large amounts of data for each measurement point. For this reason the standard VKI medium speed system of data acquisition on the PDP 11/34 is utilized. The scheme is shown in figure 3.3. All the signals, those from the LDV (two velocity components) and those from the HWA (concentration), before arrival in the ADC, are low-pass filtered at 1.5 kHz to eliminate noise (1.5 kHz is a value consistent with the response time of the concentration probe and with the value of the data rate of the LDV). The data were digitized and stored on the computer to be processed afterwards using VKI transfer function programs available on the PDP 11/34 and on the VAX.

3.2.3 Precision of the measurements

Following the standard error analysis (Ref. 9) the experimental uncertainty is of the order of 3% for the velocity measurements and of the order of 2% He in air in volume for the concentration measurements. For the power spectra computation with the FFT VKI program the frequency bandwidth is 6 Hz.

3.3 Presentation of results

3.3.1 Mean concentration measurements

The mean concentration profiles, for the 16% turbulence case, at constant x positions, are shown in figures 3.4 and 3.5 (all the data for the six cases can be found in reference 10). It can be clearly seen from these figures that in the unstable case, dissipation is increased, which is the expected result.

The same data, but plotted in terms of constant y positions, are shown in figures 3.6 and 3.7. At y positions very close to the wall, a certain flattening is observed. This can arise from the averaging effect of the probe size and also from the effect of the vertical velocity component.

3.3.2 Mean velocity measurements

For the mean velocity profiles, the most interesting observations come from the comparison of the three configurations: reference, stable and unstable. The shape of the profile itself is not very sensitive to changes in parameters of the turbulent layer or the mean external velocity.

As a typical example, compare the velocity profiles taken at a distance equal to 52.5 cm downstream from the leading edge of the plate, for a turbulence level of 3%. These profiles are shown in figure 3.8. It is evident that stratification in density influences the thickness of the boundary layer.

3.3.3 Turbulence intensities measurements

The turbulent intensity is defined as the ratio of the root-mean-square of the fluctuating part to the mean part. Figure 3.9 shows the turbulent intensity profiles of the longitudinal and vertical velocity components and of the He concentration for the same geometrical and flow conditions as

previously discussed. In the unstable case the turbulent layers are about two times the ones of the neutral condition in the first 50% of the boundary layer thickness while, outside the boundary layer thickness, they have about the same value.

In the stable stratification, near the wall (first 50% of δ), the turbulent layers remain larger than the ones of the reference case, although much smaller than the corresponding values for the unstable stratification.

3.3.4 Turbulence spectra and macroscales

The power spectral density, in terms of frequency for the fluctuating part of the concentration and of the two velocity components are also computed with the method of the fast Fourier transform. Details and results of these computations can be found in reference 10. Some spectra for a specified spatial position are shown in figure 3.9. Both stable and unstable cases are shown for the low turbulence case. There is not a great deal of difference between the two curves, although it can be said that there is a small increase in power for the unstable case, an expected trend. The difference is not, however, large enough to make any conclusive statements. The third curve is for the stable case at a higher turbulence level (16%). Here the high frequencies, representing the background turbulence, have a higher power level, of course. The other qualities of the curve remain basically unchanged.

3.4 Analysis of possible errors in concentration measurements

3.4.1 Probe size

The diameter of the probe, at its widest part, is 9 mm. Very little reliability can be placed on the measurements at $z = 0.4$ and 0.1 mm, as the disturbance to the flow is on this scale. The opening of the probe itself is 2 mm in diameter,

meaning that any measurement is an average over at least this 2 mm diameter space. Close to the wall, where the gradients are expected to be very steep, this may result in serious inaccuracies.

3.4.2 Calibration

Although an error analysis showed that the concentration can be measured to within 2% accuracy (see experimental section) inspection of figure 3.10 shows that a linear calibration curve fits the data to only about 7%. Thus, the concentration measurements cannot be expected to be better than 7% accurate.

4. NUMERICAL SIMULATION

4.1 Basic equations and simplifications

The equation to be solved numerically is (refer to equation 2.3) :

$$\frac{\partial \bar{c}}{\partial t} + \frac{\partial}{\partial x_i} \bar{c} \bar{u}_i + \frac{\partial}{\partial x_i} \overline{c' u_i'} = (1-\alpha) \frac{\partial}{\partial x_i} D_{AB} \frac{\partial \bar{c}}{\partial x_i} \quad (2.3)$$

In a two dimensional flow field, this becomes :

$$\frac{\partial \bar{c}}{\partial t} + \frac{\partial}{\partial x} \bar{u} \bar{c} + \frac{\partial}{\partial y} \bar{v} \bar{c} = \frac{\partial}{\partial x} \left(D_{AB} \frac{\partial \bar{c}}{\partial x} - \overline{u' c'} \right) + \frac{\partial}{\partial y} \left(D_{AB} \frac{\partial \bar{c}}{\partial y} - \overline{v' c'} \right) \quad (4.1)$$

The coordinate system is set with x being in the direction of the flow and y is in the vertical direction.

In the actual experiment (see Chapter 3), the exit velocity of the gas, through the porous plate, is approximately 0.02 m/s. An approximate calculation (see section 4.6.3) showed a maximum velocity contribution from gravity effects to be of the order of 0.08 m/s. This can be assumed equal to the maximum value of \bar{v} in the field (mean vertical velocity component). Thus, the third term in equation (4.1) may be neglected, yielding :

$$\frac{\partial \bar{c}}{\partial t} + \frac{\partial}{\partial x} \bar{u} \bar{c} = \frac{\partial}{\partial x} \left(D_{AB} \frac{\partial \bar{c}}{\partial x} - \overline{u' c'} \right) + \frac{\partial}{\partial y} \left(D_{AB} \frac{\partial \bar{c}}{\partial y} - \overline{v' c'} \right) \quad (4.2)$$

Ordinarily, as mentioned previously, the momentum equation is solved for the mean velocity in the horizontal direction, \bar{u} , for input into equation (4.2). But if it is assumed that the presence of the gas does not affect the mean velocity field, \bar{u} can be considered a known input, reducing the problem to that of solving one equation only, equation (4.2).

For the turbulent dispersion terms, $\overline{u'c'}$ and $\overline{v'c'}$, the gradient flux model is used, i.e.,

$$\overline{u'c'} = -K_x \frac{\partial \bar{c}}{\partial x} \quad (4.3)$$

$$\overline{v'c'} = -K_y \frac{\partial \bar{c}}{\partial y}$$

where K_x and K_y are known as the turbulent diffusivities in the x and y directions, respectively. Then equation (4.2) can be written as :

$$\frac{\partial c}{\partial t} + \frac{\partial}{\partial x} \bar{u}\bar{c} = \frac{\partial}{\partial x} \left[(D_{AB} + K_x) \frac{\partial \bar{c}}{\partial x} \right] + \frac{\partial}{\partial y} \left[(D_{AB} + K_y) \frac{\partial \bar{c}}{\partial y} \right] \quad (4.4)$$

Generally, the turbulent diffusivity is much greater than the molecular diffusivity, such that D_{AB} can be neglected with respect to K_x or K_y in equation (4.4). Thus, the equation to be solved is :

$$\frac{\partial \bar{c}}{\partial t} + \frac{\partial}{\partial x} \bar{u}\bar{c} = \frac{\partial}{\partial x} \left[K_x \frac{\partial \bar{c}}{\partial x} \right] + \frac{\partial}{\partial y} \left[K_y \frac{\partial \bar{c}}{\partial y} \right] \quad (4.5)$$

A summary of the assumptions is as follows :

1. Two dimensional flow field,
2. Negligible mean velocity in the vertical direction, \bar{v} .
3. Mean velocity in the horizontal direction, \bar{u} , not changed by the presence of the gas.
4. Gradient flux model for the turbulent dispersion terms.
5. Molecular diffusivity negligible.

The severity of each of these assumptions will be discussed in turn.

The first assumption, that of a two dimensional flow field, infers that the tunnel can be considered infinite in width. Thus, it is best at the center of the tunnel, farthest away from the walls. That is, the walls induce three dimensional effects. In fact, the measurements were taken very near the center of the tunnel. Unfortunately, there was no time to make measurements to verify the two dimensional character of the flow.

In assuming that \bar{v} can be neglected, the term dropped from equation (4.1) is $\bar{v}\partial c/\partial y$. As $\partial c/\partial y$ can be very large, this assumption is actually not very good. It is expected that \bar{v} will become zero some short distance from the wall, so the assumption causes large errors near the wall, and that error decreases as the distance from the wall increases. The actual value of \bar{v} was not measured anywhere in the field.

The real effect that the gas has on the mean horizontal velocity, \bar{u} , can be clearly seen in the experimental measurements shown in section 3.3.2. Again, the assumption is not valid very near the wall, but fairly good a small distance from the wall.

There is no indication, a priori, as to the applicability of the gradient flux model for the turbulent dispersion terms in this case. The assumption states, simply, that the diffusion terms can be expressed as a function of the gradient of the average concentration.

The molecular diffusivity of some typical pollutants is shown in table 4.1. From measurements (see Ref. 1), the turbulent diffusivity in the atmosphere is usually on the order of $1 \text{ m}^2/\text{s}$. Hence, this assumption is quite good.

4.2 Discretizations

The first step in the discretization of equation (4.5) is the representation of $\partial c/\partial t$:

$$\frac{\partial \bar{c}}{\partial t} = \frac{\bar{c}_{ij}^{\ell+1} - \bar{c}_{ij}^{\ell}}{\Delta t} \quad (4.6)$$

To use the "delta" representation (Ref. 3), we introduce the parameter δ_{ij} :

$$\delta_{ij} = \bar{c}_{ij}^{\ell+1} - \bar{c}_{ij}^{\ell} \quad (4.7)$$

Equation (4.5) can thus be written as :

$$\frac{\delta_{ij}}{\Delta t} + \frac{\partial}{\partial x} \left[\bar{u} \bar{c} - K_x \frac{\partial \bar{c}}{\partial x} \right] + \frac{\partial}{\partial y} \left[-K_y \frac{\partial \bar{c}}{\partial y} \right] = 0 \quad (4.8)$$

The solution is sought for the steady state; therefore, a fully implicit scheme may be used :

$$\frac{\delta_{ij}}{\Delta t} + \left[\frac{\partial}{\partial x} \left[\bar{u} \bar{c} - K_x \frac{\partial \bar{c}}{\partial x} \right] \right]_{ij}^{\ell+1} + \left[\frac{\partial}{\partial y} \left[-K_y \frac{\partial \bar{c}}{\partial y} \right] \right]_{ij}^{\ell+1} = 0 \quad (4.9)$$

Equation (4.9) can be written in operator notation :

$$\frac{\delta_{ij}}{\Delta t} + \left[\frac{\partial}{\partial x} \left[\bar{u} - K_x \frac{\partial}{\partial x} \right] \right] \bar{c}_{ij}^{\ell+1} + \left[\frac{\partial}{\partial y} \left[-K_y \frac{\partial}{\partial y} \right] \right] \bar{c}_{ij}^{\ell+1} = 0 \quad (4.10)$$

Note from equation (4.7) :

$$\bar{c}_{ij}^{\ell+1} = \delta_{ij} + \bar{c}_{ij}^{\ell} \quad (4.11)$$

Substitution of equation (4.11) into (4.10) and rearrangement yields :

$$\left[1 + \Delta t \left[\frac{\partial}{\partial x} \left(\bar{u} - K_x \frac{\partial}{\partial x} \right) \right] + \Delta t \left[\frac{\partial}{\partial y} \left(-K_y \frac{\partial}{\partial y} \right) \right] \right] \delta_{ij} =$$

$$= \Delta t \frac{\partial}{\partial y} K_y \frac{\partial}{\partial y} \bar{c}_{ij}^L - \Delta t \frac{\partial}{\partial x} \bar{u} \bar{c}_{ij}^L + \Delta t \frac{\partial}{\partial x} K_x \frac{\partial}{\partial x} \bar{c}_{ij}^L \quad (4.12)$$

The left-hand side of equation (4.12) can be factored after the manner of Beam and Warming (Ref. 3) with an error of order Δt^2 :

$$\left[1 + \Delta t \left[\frac{\partial}{\partial x} \left(\bar{u} - K_x \frac{\partial}{\partial x} \right) \right] \right] \left[1 + \Delta t \left[\frac{\partial}{\partial y} \left(-K_y \frac{\partial}{\partial y} \right) \right] \right] \delta_{ij} + O(\Delta t^2) = \text{RHS} \quad (4.13)$$

(Note that RHS refers to the right hand side of equation 4.12). Equation (4.13) can then be solved in two separated parts :

$$\left[1 + \Delta t \left[\frac{\partial}{\partial y} \left(-K_y \frac{\partial}{\partial y} \right) \right] \right] \delta_{ij} = f_{ij} \quad (4.14)$$

and

$$\left[1 + \Delta t \left[\frac{\partial}{\partial x} \left(\bar{u} - K_x \frac{\partial}{\partial x} \right) \right] \right] f_{ij} = \text{RHS} \quad (4.15)$$

Equation (4.15) is solved first, for f_{ij} ; then equation (4.14) may be solved for δ_{ij} .

The diffusive terms are discretized in the following manner :

$$\Delta t \frac{\partial}{\partial y} \left(K_y \frac{\partial}{\partial y} \right) \delta_{ij} = \frac{\Delta t}{\Delta y^*} \left(K_y \frac{\partial \delta}{\partial y} \Big|_{i,j+1/2} - K_y \frac{\partial \delta}{\partial y} \Big|_{i,j-1/2} \right) \quad (4.16)$$

If h is a stretching function that describes the position y ,

$$y = h(\bar{y}) \quad (4.17)$$

where $\Delta \bar{y}$ will define an equally spaced grid. By these definitions

$$\Delta y^* = \left(h'_j + h'_{j+1} \right) \frac{\Delta \bar{y}}{2} \quad (4.18)$$

where

$$h'_j = \frac{h_j - h_{j-1}}{\Delta \bar{y}} \quad (4.19)$$

Using the same notation

$$K_y \frac{\partial \delta}{\partial y} \Big|_{i,j+1/2} = \left(\frac{K_{y_{i,j+1}} + K_{y_{ij}}}{2} \right) \left(\frac{\delta_{i,j+1} - \delta_{ij}}{h'_{j+1} \Delta \bar{y}} \right) \quad (4.20)$$

and

$$K_y \frac{\partial \delta}{\partial y} \Big|_{i,j-1/2} = \left(\frac{K_{y_{ij}} + K_{y_{i,j-1}}}{2} \right) \left(\frac{\delta_{ij} - \delta_{i,j-1}}{h'_j \Delta \bar{y}} \right) \quad (4.21)$$

Substitution of equations (4.18), (4.20) and (4.21) into equation (4.16) yields :

$$\Delta t \frac{\partial}{\partial y} \left[K_y \frac{\partial}{\partial y} \right] \delta_{ij} = \frac{\Delta t}{\Delta \bar{y}^2} \frac{(K_{y_{i,j+1}} + K_{y_{ij}})(\delta_{i,j+1} - \delta_{ij})}{h'_{j+1}(h'_j + h'_{j+1})} \quad (4.22)$$

$$+ \frac{\Delta t}{\Delta \bar{y}^2} \frac{(K_{y_{ij}} + K_{y_{i,j-1}})(\delta_{ij} - \delta_{i,j-1})}{h'_j(h'_j + h'_{j+1})}$$

Each diffusive term is discretized in like manner.

The following procedure is used to discretize the convective terms. The stretching function is represented by :

$$x = g(\bar{x}) \quad (4.23)$$

and behaves in like manner as $h(\bar{y})$. Thus

$$\Delta t \left(\frac{\partial \bar{u} \bar{c}}{\partial x} \right)_{ij}^{\ell} = \Delta t \left(\frac{1}{g'} \frac{\partial}{\partial \bar{x}} \bar{u} \bar{c} \right)_{ij}^{\ell}$$

A scheme is utilized that is partially centered and partially excentered, using a proportionality factor, λ :

$$\Delta t \left(\frac{\partial \bar{u} \bar{c}}{\partial x} \right)_{ij}^{\ell} = \lambda \Delta t \left[\frac{(\bar{u} \bar{c})_{ij}^{\ell} - (\bar{u} \bar{c})_{i-1,j}^{\ell}}{g'_i \Delta \bar{x}} \right] \quad (4.25)$$

$$+ (1-\lambda) \Delta t \left[\frac{(\bar{u} \bar{c})_{i+1,j}^{\ell} - (\bar{u} \bar{c})_{i-1,j}^{\ell}}{\Delta \bar{x} (g'_{i+1} + g'_i)} \right]$$

The convective term in f_{ij} is discretized in the same way. Making the appropriate substitutions, the fully discretized forms of equations (4.14) and (4.15) are :

$$\delta_{ij} + \frac{\Delta t}{\Delta \bar{y}^2} \left[\frac{(K_{y_{i,j+1}} + K_{y_{ij}})(\delta_{i,j+1} - \delta_{ij})}{h'_{j+1}(h'_j + h'_{j+1})} + \frac{(K_{y_{ij}} + K_{y_{i,j-1}})(\delta_{ij} - \delta_{i,j-1})}{h'_j(h'_j + h'_{j+1})} \right] = f_{ij} \quad (4.26)$$

$$f_{ij} + \frac{\Delta t}{\Delta \bar{x}} \left[\frac{\lambda[(\bar{u}f)_{ij} - (\bar{u}f)_{i-1,j}]}{g'_i} + \frac{(1-\lambda)(\bar{u}f)_{i+1,j} - (\bar{u}f)_{i-1,j}}{g'_{i+1} + g'_i} \right] - \frac{\Delta t}{\Delta \bar{x}^2} \left[\frac{(K_{x_{i+1,j}} + K_{x_{ij}})(f_{i+1,j} - f_{ij})}{g'_{i+1}(g'_i + g'_{i+1})} + \frac{(K_{x_{ij}} + K_{x_{i-1,j}})(f_{ij} - f_{i-1,j})}{g'_i(g'_i + g'_{i+1})} \right] = R H S \quad (4.27)$$

$$\begin{aligned}
 \text{RHS} = & \frac{\Delta t}{\Delta \bar{y}^2} \frac{(K_{y_{ij}} + K_{y_{i,j-1}})}{h'_j(h'_{j+1} + h'_j)} \bar{c}_{i,j-1}^\ell + \left[- \frac{\Delta t}{\Delta \bar{y}^2} \frac{(K_{y_{i,j+1}} + K_{y_{ij}})}{h'_{j+1}(h'_{j+1} + h'_j)} \right. \\
 & - \frac{\lambda \Delta t}{g'_i \Delta \bar{x}} \bar{u}_{ij}^\ell - \frac{\Delta t}{\Delta \bar{y}^2} \frac{(K_{y_{ij}} + K_{y_{i,j-1}})}{h'_j(h'_{j+1} + h'_j)} - \frac{\Delta t}{\Delta \bar{x}^2} \frac{(K_{x_{i+1,j}} + K_{x_{ij}})}{(g'_{i+1} + g'_i)g'_i} \\
 & \left. - \frac{\Delta t}{\Delta \bar{x}^2} \frac{(K_{x_{ij}} + K_{x_{i-1,j}})}{g'_i(g'_{i+1} + g'_i)} \right] \bar{c}_{ij}^\ell + \frac{\Delta t}{\Delta \bar{y}^2} \frac{(K_{y_{i,j+1}} + K_{y_{ij}})}{(h'_{j+1}(h'_{j+1} + h'_j))} \bar{c}_{i,j+1}^\ell \\
 & + \left[\frac{\lambda \Delta t \bar{u}_{i-1,j}^\ell}{g'_i \Delta \bar{x}} + \frac{(1-\lambda) \Delta t \bar{u}_{i-1,j}^\ell}{\Delta \bar{x}(g'_{i+1} + g'_i)} + \frac{\Delta t}{\Delta \bar{x}^2} \frac{(K_{x_{ij}} + K_{x_{i-1,j}})}{g'_i(g'_{i+1} + g'_i)} \right] \bar{c}_{i-1,j}^\ell \\
 & + \left[- \frac{(1-\lambda) \Delta t \bar{u}_{i+1,j}^\ell}{\Delta \bar{x}(g'_{i+1} + g'_i)} + \frac{\Delta t}{\Delta \bar{x}^2} \frac{(K_{x_{i+1,j}} + K_{x_{i,j}})}{(g'_{i+1} + g'_i)g'_{i+1}} \right] \bar{c}_{i+1,j}^\ell
 \end{aligned}$$

4.3 Grid generation

The computational field is a rectangular slice in the two dimensional plane. The boundaries at $y=0$ and $y=1$ represent the upper and lower walls of the wind tunnel. The boundary at $x=0$ is the inflow boundary, taken a distance, b (which is variable), upstream of the plate source. The boundary at $x=1$ is the outflow boundary, taken a large distance (also variable) downstream of the plate.

In the vertical (y -axis) direction, the concentration gradient is most pronounced at the injection side, i.e., near $y=0$. Therefore, a finer mesh is required there than in the rest of the field. Let the stretching function be represented by $h(\bar{y})$, where \bar{y} is the transformed coordinate system. A parabolic stretching function was chosen as follows :

$$h = 2 \bar{y}^2/3 + \bar{y}/3$$

In this way, the step size at $y=0$ is one-fifth that at the lower boundary ($y=1$).

In the horizontal (x -axis) direction, there are sharp gradients at the two plate edges. Let $g(\bar{x})$ represent the stretching function in the x -direction. A cosine function was chosen from $x=0$ to the plate trailing edge. Then a parabolic function is used from the trailing edge to the end of the field ($x=1$). The resulting function is as follows :

$$g(\bar{x}) = \begin{cases} -\frac{350a}{L} \cos \left[\frac{\pi L}{175} \left(\bar{x} - \frac{b}{L} - \frac{87.5}{L} \right) \right] & g < \frac{b+350}{L} \\ + 3a \left(\bar{x} - \frac{b}{L} - \frac{87.5}{L} \right) + d & \\ m\bar{x}^2 + e\bar{x} + f & g > \frac{b+350}{L} \end{cases} \quad (4.30)$$

where

L = the length of the computational field in mm

b = the position of the plate leading edge in mm

a, d, m, e, f = constants determined by the desired range of step sizes and total number of steps.

The constants were chosen such that the step size in the center of the plate is five times that at the edges. The grid itself is shown, with various parameters (indicated on the figures) in figures 4.1 to 4.3.

4.4 Boundary conditions

4.4.1 Upper and lower walls

On both upper and lower walls, the basic equations for the inner points are solved. Since centered discretizations in the vertical direction are used, the basic equations use non-existent points. The value of the concentration at the non-existent points can be replaced by the value of the concentration at the points in the inner field that are the "reflection" of the non-existent points, thus making a statement of wall impermeability. With this assumption, the equations as discretized in section 4.2 can be solved on the boundaries.

At the porous wall section, the concentration is set at a constant value, $\bar{c} = 0.5$. This value was chosen as the porous plate has a porosity of 50%. Thus $\bar{c} = 0.5$ over the length of the plate should be an accurate description of the mass flow across the plate, distributed evenly across the source plate. Thus, it should be accurate on a global scale, but not very near to the plate itself.

4.4.2 Inflow and outflow

For the inflow boundary ($x=0$), a strong boundary condition is used, i.e., $\bar{c} = 0$. This poses no problems if b , the distance of the plate leading edge from the computational boundary, is taken large enough.

The boundary condition applied at the outflow ($x=1$) is on the first derivative. That is,

$$\partial \bar{c} / \partial x = 0. \quad (4.31)$$

This is only true at a sufficient distance downstream from the plate trailing edge.

4.5 Test case

To check the scheme, a problem is solved for which the exact solution is known. This is done by modifying the field slightly. The modified case is one where the plate ($\bar{c} = 1$) extends until $x = 1$. Then from equation (4.5) :

$$\frac{\partial \bar{c}}{\partial t} + \frac{\partial}{\partial x} \bar{u} \bar{c} = \frac{\partial}{\partial x} K_x \frac{\partial \bar{c}}{\partial x} + \frac{\partial}{\partial y} K_y \frac{\partial \bar{c}}{\partial y} \quad (4.5)$$

Assume that :

- $K_x = K_y = K$
- Steady state, i.e., $\partial c / \partial t = 0$
- $\bar{u} = 1$
- $K = \text{constant}$, i.e., $\partial K / \partial x_i = 0$

Then equation (4.5) is reduced to :

$$\frac{\partial \bar{c}}{\partial x} = K \frac{\partial^2 \bar{c}}{\partial x^2} + K \frac{\partial^2 \bar{c}}{\partial y^2} \quad (4.32)$$

If K is small with respect to unity, then :

$$K \frac{\partial^2 \bar{c}}{\partial x^2} \ll \frac{\partial \bar{c}}{\partial x} \quad (4.33)$$

and

$$\frac{\partial \bar{c}}{\partial x} = K \frac{\partial^2 \bar{c}}{\partial y^2} \quad (4.34)$$

Equation (4.34) can be solved analytically with the following boundary conditions :

$x = 0$ implies that $\bar{c} = 0$ for all y

$y = 0$ implies that $\bar{c} = 1$ for all $x > 0$ (4.35)

$y = \infty$ implies that $\bar{c} = 0$ for all $x > 0$

Note that the last boundary condition can only be used if there is no interaction between the concentration field and the far wall (at $y = 1$). The experimental data shown in chapter 3 confirm that this is an acceptable boundary condition for the range of K in which the solution shall be made. Solving for \bar{c} :

$$\bar{c} = 1 - \frac{2}{\sqrt{\pi}} \int_0^{y/\sqrt{4Kx}} e^{-\eta^2} d\eta \quad (4.36)$$

or

$$\bar{c} = 1 - \operatorname{erf} \left[\frac{y}{\sqrt{4Kx}} \right] \quad (4.37)$$

Some lines of constant concentration are shown in figure 4.9 for $K = 0.01$. The numerical program was modified to use the boundary conditions (4.35) and the resulting solution is also shown in figure 4.4. It can be seen that the only discrepancy between the two solutions is at the plate leading edge. The small error seen here is due to the diffusion in the x -direction, which is neglected in the analytic solution. It appears upstream from the plate, as there is no convection upstream, thus expression (4.33) is not valid in this region.

4.6 Evaluation of expected error in scheme

4.6.1 Upwinding

To avoid the appearance of "wiggles" in the solution originating at the boundary, a partially "upwinded" discretization is used for the convective terms. Assuming, for simplicity, that the first derivative of the stretching function is equal to unity (i.e., constant step size), equation 4.26 can be written as :

$$\Delta t \left(\frac{\partial \bar{u}\bar{c}}{\partial x} \right) = \frac{\Delta t(1-\lambda)}{2\Delta x} \left[(\bar{u}\bar{c})_{i+1,j} - (\bar{u}\bar{c})_{i-1,j} \right] + \frac{\Delta t\lambda}{\Delta x} \left[(\bar{u}\bar{c})_{ij} - (\bar{u}\bar{c})_{i-1,j} \right]$$

Expanding and simplifying

$$\begin{aligned} \Delta t \left(\frac{\partial \bar{u}\bar{c}}{\partial x} \right) &= \frac{\Delta t(1-\lambda)}{2\Delta x} \left[2\Delta x \frac{\partial \bar{u}\bar{c}}{\partial x} + 0(\Delta x^3) \right] + \frac{\Delta t\lambda}{\Delta x} \left[\Delta x \frac{\partial \bar{u}\bar{c}}{\partial x} + \frac{\Delta x^2}{2} \frac{\partial^2 \bar{u}\bar{c}}{\partial x^2} + 0(\Delta x^3) \right] \\ &= \Delta t \frac{\partial \bar{u}\bar{c}}{\partial x} + \frac{\Delta t\lambda\Delta x}{2} \frac{\partial^2 \bar{u}\bar{c}}{\partial x^2} \end{aligned} \quad (4.39)$$

Thus, the process of upwinding introduces an effective diffusion, with a coefficient of magnitude $\lambda \Delta x / 2$. In any calculation using this scheme, the magnitude of this term should be evaluated with respect to the physical diffusivity of the problem. Obviously, λ should be kept as small as possible.

The minimum total diffusivity that the scheme can handle is of the order of 10^{-3} . Thus, for accurate problem solutions the physical diffusivity should be of order 10^{-3} or greater. That is, the scheme is inapplicable for very small physical diffusivity.

4.6.2 Error introduced by the stretching function

Consider the simplified equation with convection and diffusion (i.e., $K = \text{const.}$, $\bar{u} = 1.$), and stretching functions in x and y as previously defined. The basic equation, in physical space, is, at steady state :

$$\frac{\partial \bar{c}}{\partial x} = K \frac{\partial^2 \bar{c}}{\partial x^2} + K \frac{\partial^2 \bar{c}}{\partial y^2} \quad (4.40)$$

This becomes, in the transformed space :

$$\frac{1}{g'} \frac{\partial \bar{c}}{\partial \bar{x}} = \frac{K}{g'} \frac{\partial}{\partial \bar{x}} \left(\frac{1}{g'} \frac{\partial \bar{c}}{\partial \bar{x}} \right) + \frac{K}{h'} \frac{\partial}{\partial y} \left(\frac{1}{h'} \frac{\partial \bar{c}}{\partial y} \right) \quad (4.41)$$

If a centered discretization is used for the convective term,

$$\frac{\partial \bar{c}}{\partial \bar{x}} = \frac{\bar{c}_{i+1,j} - \bar{c}_{i-1,j}}{2\Delta \bar{x}} \quad (4.42)$$

Expanded in physical space,

$$\bar{c}_{i+1,j} = \bar{c}_{ij+\Delta x} \frac{\partial \bar{c}}{\partial x} + \frac{\Delta x^2}{2} \frac{\partial^2 \bar{c}}{\partial x^2} + \text{HOT} \quad (4.43)$$

$$\bar{c}_{i-1,j} = \bar{c}_{ij+\Delta x} \frac{\partial \bar{c}}{\partial x} + \frac{\Delta x^2}{2} \frac{\partial^2 \bar{c}}{\partial x^2} + \text{HOT}$$

and equation (4.42) becomes :

$$\frac{\partial \bar{c}}{\partial x} = \left(\frac{g_{i+1} - g_{i-1}}{2\Delta \bar{x}} \right) \frac{\partial \bar{c}}{\partial x} + \frac{1}{2\Delta \bar{x}} \left[\frac{(g_{i+1} - g_i)^2}{2} - \frac{(g_i - g_{i-1})^2}{2} \right] \frac{\partial^2 \bar{c}}{\partial x^2} \quad (4.44)$$

The stretching function can also be expanded, in the transformed space, as :

$$g_{i+1} = g_i + \Delta \bar{x} g_i' + \frac{\Delta \bar{x}^2}{2} g_i'' + \text{HOT} \quad (4.45)$$

$$g_{i-1} = g_i - \Delta \bar{x} g_i' + \frac{\Delta \bar{x}^2}{2} g_i'' + \text{HOT}$$

and equation (4.44) becomes :

$$\frac{\partial \bar{c}}{\partial x} = g' \frac{\partial \bar{c}}{\partial x} + \frac{\Delta \bar{x}^2 g' g''}{2} \frac{\partial^2 \bar{c}}{\partial x^2} \quad (4.46)$$

Thus,

$$\frac{1}{g'} \frac{\partial \bar{c}}{\partial x} = \frac{\partial \bar{c}}{\partial x} + \frac{\Delta \bar{x}^2 g''}{2} \frac{\partial^2 \bar{c}}{\partial x^2} \quad (4.47)$$

It is thus seen that due to the stretching function, a diffusion term is added with effective diffusivity of magnitude $\Delta x^2 g''/2$. This can be positive or negative, depending on the sign of g'' . With the stretching function as shown in section 4.3, and 60 steps, the maximum value of this effective diffusivity is 10^{-3} . So, again, the conclusion is reached that this scheme is not accurate for physical diffusivity less than 10^{-3} .

4.6.3 Approximation of velocity due to gravity effects

In the code as written, the effect of gravity was not directly modelled, but the coefficient of turbulent diffusivity was considered to include the gravity effects. This introduces some error, obviously, especially when D_x and D_y are taken as constant through the field. That is, if the D_y is increased to represent an increased diffusivity due to gravity effects, the fact that it is increased in both positive and negative directions will result in an error for the physical modelling of the problem. A simple approximation of the velocity that could be caused by the density variation was made to get an idea of the magnitude of this error.

Consider a two dimensional "lump" of fluid of dimensions $dx dy$ and density ρ_1 . If the surrounding fluid has a density ρ_s , the potential energy contained in the fluid "lump" can be represented by :

$$P = (\rho_1 - \rho_s) g dy$$

where g is the acceleration due to gravity. The kinetic energy can be represented by

$$K = \rho_1 v^2 / 2$$

If all the potential energy is converted to kinetic energy, and there is considered to be no drag forces or viscous effects (thus a high estimation of the velocity), the energy balance can be expressed as

$$(\rho_1 - \rho_s) g dy = \rho_1 v^2 / 2$$

Solving for v ,

$$v = \left[2(\rho_1 - \rho_s) g dy / \rho_1 \right]^{1/2}$$

The concentration gradients are the highest in the y direction near the porous plate, so this equation was used to calculate the velocity at several positions near the plate. The maximum value of v was found at the leading edge of the plate, where v had a value of 0.08 m/s. At the trailing edge v was found to be 0.04 m/s. This is on the order of 1% of the free stream velocity, which is the same order of magnitude as the minimum turbulence level. Thus, we can expect that modelling the gravity effects through the diffusivity will give reasonable results.

4.7 Presentation of results

4.7.1 Numerical results

Several runs of the numerical code were made to see the effect of the pertinent parameters. Figure 4.5 is a comparison of two separate runs at two stations downstream from the plate source. All the parameters are the same excepting the diffusivity in the vertical direction, D_y . The effect that increased diffusivity in the vertical direction has on the concentration profile can be clearly seen. The maximum concentration (near the wall) is only minimally affected, but the concentration is much higher for the higher diffusion case as y increases. It is proposed that "instability" (defined in the experimental section) would be reflected numerically by an increased vertical diffusivity. In fact, the experimental data, as evidenced by figures 3.4 (j) and 3.5(h) reflects the same trend as observed in figure 4.5. In figure 4.6, the effect of varying u_{∞} directly is illustrated. The equations have been non-dimensionalized and the characteristic velocity was chosen as u_{∞} . Thus the U_{∞} , non dimensionalized, is always equal to 1 and the effect of changing the main stream velocity is reflected in the value of the non dimensionalized diffusivities, $D_x = D_x/Ux$ and $D_y = D_y/Ux$, where D_x and D_y are the non dimensionalised diffusivities, x is the characteristic

length scale, and U is u_{∞} . Thus, to vary the physical main stream velocity, it is necessary to change the values of the diffusivities in both directions. This has been done to generate the curves in figure 4.6. The difference between the two cases is greatest far away from the wall, while in the experimental data, the effect of increasing the velocity was felt the most very near the wall. From this it can be concluded that the change in main stream velocity also has an effect on the diffusivity that is not modelled in this program, which runs only at constant diffusivity.

4.7.2 Comparison of experimental and numerical results

In figures 4.7 and 4.8, a comparison of the experimental and numerical results is made. In figure 4.7a comparisons are made with the experimental data when the turbulent intensity is changed. The diffusion coefficients are normally assumed to be proportional to the turbulent intensities. Figure 4.8 supports this assumption, as both diffusion coefficients are doubled when the turbulent intensity is doubled and the agreement with experiment is fair. Figure 4.7b shows a comparison of calculation with experiment for stable and unstable cases. For the unstable case, the diffusivity in the vertical direction is taken as larger than the diffusivity in the horizontal direction. For the stable case, D_y is smaller than D_x by a factor of 5, to be consistent with the hypothesis that the effect of gravity can be modelled by changes in the vertical diffusivity. To model the effect of changing main stream velocity, for the stable case, fairly good results were obtained by simply halving the diffusivities in both directions to represent a doubled velocity, as shown in figure 4.8. In traditional heavy gas models using the Gaussian approach, it is quite common to use σ_y , which is proportional to the diffusivity in the vertical direction, increased by a factor of 5 from that which has been empirically determined for a neutral gas to account for the gravity effects. These calculations show that that is actually quite a good approximation.

5. CONCLUSIONS

The comparison of the experimental data with the numerical model revealed that even with such a simple model for the turbulent diffusion terms, the important trends can be predicted. In particular, an increase in the main stream velocity is represented numerically by a decrease in both diffusion coefficients. It was also verified that gravity effects can be represented by a change in the vertical diffusion coefficient. For the "heavy" gas situation, the ratio of D_y to D_x for good agreement with the experimental data was found to be on the order of 5, which is the commonly-used value for this ratio. And, finally, an increase in turbulent intensity of the flow is well represented by an increase in the diffusion coefficients. The relationship is directly proportional, as is traditionally assumed.

6. SUGGESTIONS FOR FUTURE STUDY

6.1 Experimental

Experimental investigation of the inaccuracies in the use of the concentration probe near the wall should be made. Also, the mean vertical velocity component should be measured. The characteristics of the probe indicate that the experiment should be made with adjustments in the flow parameters such that the measurement field is extended further away from the wall. Also, the two dimensionality of the flow field should be measured.

6.2 Numerical

The diffusivity as used in this code was constant throughout the computational field. The modelization of this diffusivity with respect to local concentration or local turbulent intensity should produce improved results. For the case where gravity effects are important, a way to incorporate these effects into the calculation of the vertical coefficient of diffusion should be formulated.

The numerical code could be extended to three dimensions. This would mean solving the factored equation in three sweeps instead of two.

A similar program can be used to solve the transport equation for second and higher moments, to achieve the final result of the probability density function of the concentration at each point in the field.

REFERENCES

1. SLADE, D.H. (Ed.): Meteorology and atomic energy. U.S. Atomic Energy Commission, July 1968.
2. RAJ, P.K.: Heavy gas dispersion. A state-of-the-art review of the experimental results and models. In: "Heavy Gas Dispersion", VKI LS 1982-03, March 1982.
3. WARMING, R.F. & BEAM, R.M.: On the construction and application of implicit factored schemes for conservation laws. SIAM-AMS Proceeding, Vol. 11, 1978.
4. BIRD, R.B.; STEWART, W.E.; LIGHTFOOT, E.N.: Transport phenomena. New York, John Wiley & Sons Inc., 1960.
5. TROLINGER, J.D.: Laser instrumentation for flow field diagnostics. AGARDograph 186, 1974.
6. OLIVARI, D. & COLIN, P.: Three applications of hot wire techniques for fluid dynamics measurements. ICIASF'71, pp 173-184. Also VKI Preprint 1971-3.
7. TAN-ATICHAT, J.; NAGIB, H.M.; LOEHRKE, R.I.: Interaction of free stream turbulence with screens and grids. A balance between turbulent scales. J. Fluid Mechanics, Vol. 114, January 1982, pp 501-528.
8. LOURENÇO, L.; BORREGO, C.; RIETHMULLER, M.L.: Simultaneous two dimensional measurements with one colour laser doppler velocimeter. VKI TM 28, June 1980.
9. KLINE, S.J. & McCLINTOCK, F.A.: Uncertainties in single-sample experiments. Mechanical Engineering, Vol. 75, No. 1, January 1953, pp 3-9.
10. TORDELLA, D.: Effect of gravity forces on turbulence development. VKI PR 1983-26, June 1983.

	Grid 1	Grid 2	Grid 3	Perforated plate PP
wire diameter [mm]	0.16	0.5	0.16	6.35
material	steel	steel	steel	steel
solidity σ	.25	.44	.30	0.42
pressure drop coefficient $K = \Delta p / \frac{1}{2} \rho u_{\infty}^2$.77	1.1	.87	1.5
thickness [mm]	0.16	0.5	0.87	1.5
mesh [mm]	0.79	1.98	0.96	8
mesh Reynolds number $Re_M = \frac{u_{\infty} M}{\nu}$ $u_{\infty} = 3 \text{ m/s}$	158	396	192	2300
wire diameter Reynolds number $Re_D = \frac{u_{\infty} d}{\nu}$ $u_{\infty} = 3 \text{ m/s}$	32	105	32	

TABLE 3.1 : TURBULENCE MANIPULATOR CHARACTERISTICS



FREQUENCY SHIFT OF THE VERTICAL BEAMS = 21 MH

PINHOLE DIAMETER = 50 μm

DIMENSION OF THE PROBE VOLUME

horizontal beams $\Delta x = .268 \text{ mm}$, $\Delta y = .268 \text{ mm}$, $\Delta z = 8.9$

vertical beams $\Delta x = .268 \text{ mm}$, $\Delta y = .268 \text{ mm}$, $\Delta z = 3.6$

NUMBER OF FRINGES INSIDE THE PROBE VOLUME

horizontal beams 25

vertical beams 63

INTERFRINGE DISTANCE

horizontal beams $10.54 \cdot 10^{-6} \text{ m}$

vertical beams $4.2 \cdot 10^{-6}$

BAND PASS FILTER

horizontal velocity component 30 KH - 1 MH

vertical velocity component 1 MH - 3 MH

TABLE 3.2 - PARAMETERS OF THE LDV OPTICAL SYSTEM

Gas Pair	Temp (°K)	D_{AB} m ² /s
CO ₂ -N ₂ O	273.2	9.6×10^{-6}
CO ₂ -CO	273.2	1.39×10^{-5}
CO ₂ -N ₂	273.2	1.44×10^{-5}
A _r -O ₂	293.2	2.0×10^{-5}
H ₂ -SF ₆	298.2	4.2×10^{-5}
H ₂ -CH ₄	298.2	7.3×10^{-5}

TABLE 4.1 - EXPERIMENTAL DIFFUSIVITIES OF SOME DILUTE GAS PAIRS
(pressure 1 atm), Ref. 4, p 503.

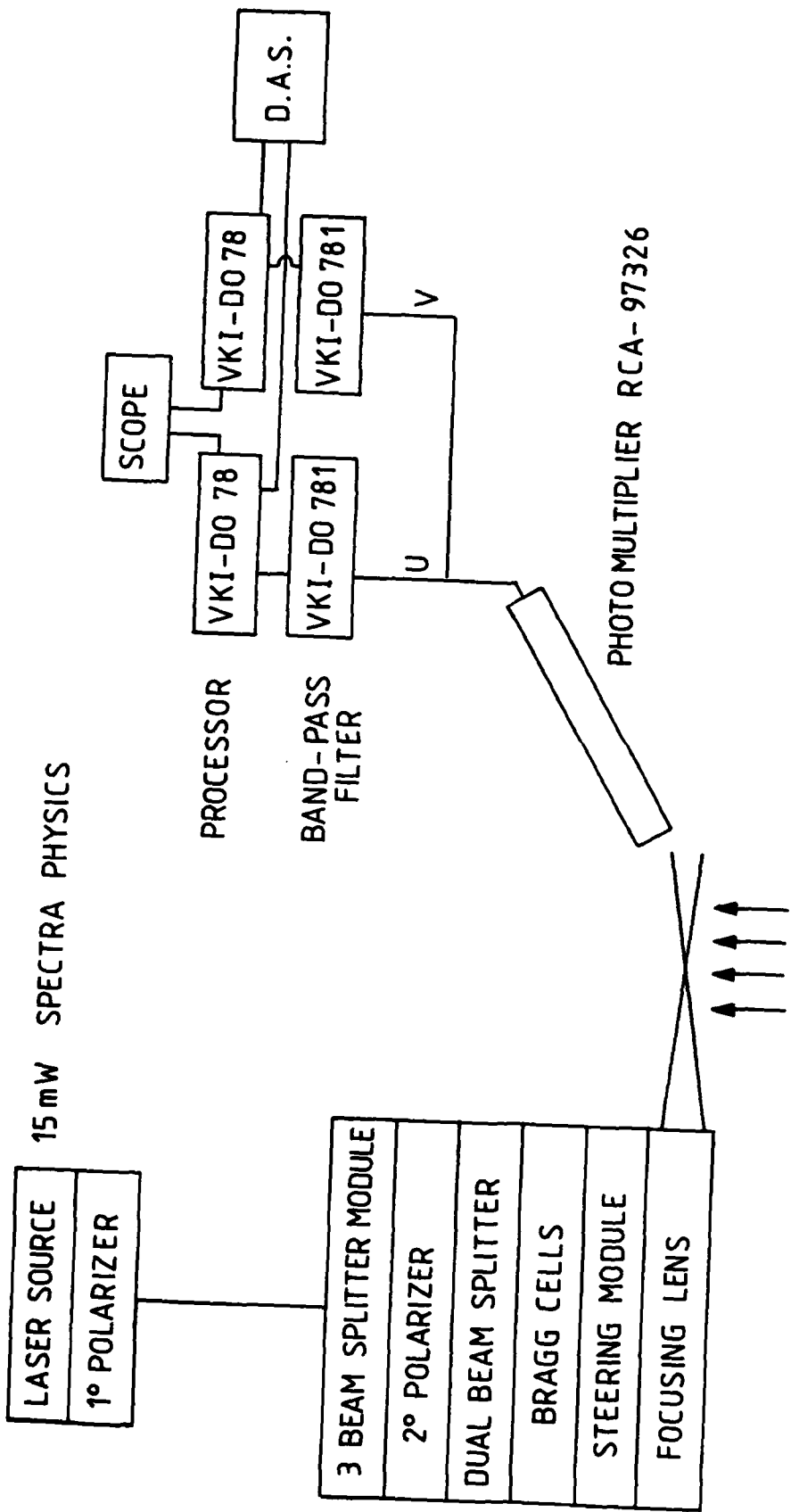


FIG. 3.1 - APPARATUS FOR VELOCITY MEASUREMENTS WITH LASER DOPPLER ANEMOMETER



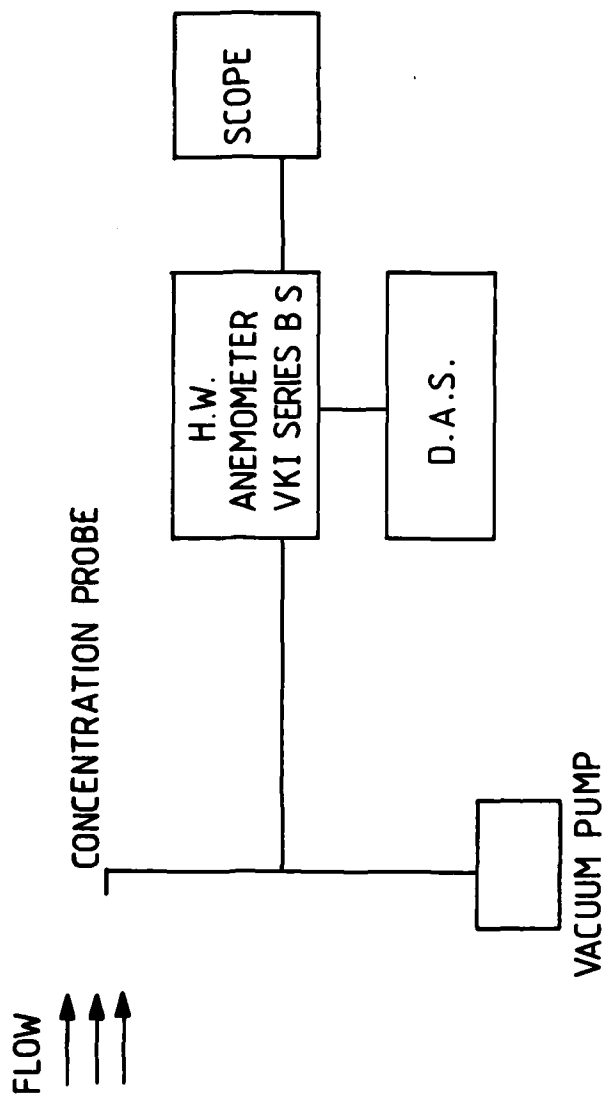


FIG. 3.2 - APPARATUS FOR CONCENTRATION MEASUREMENTS

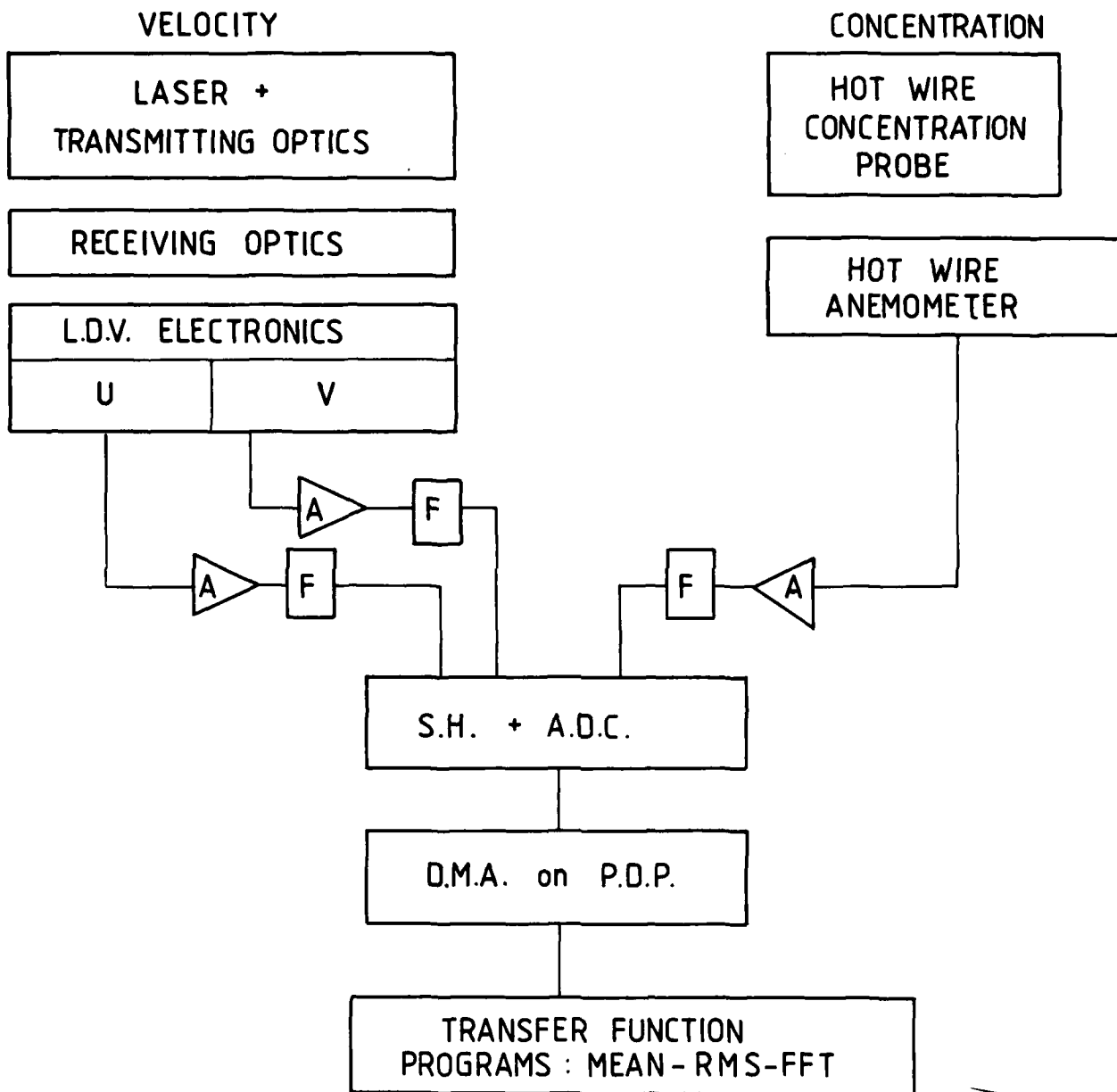


FIG. 3.3- MEASUREMENT CHAIN AND DATA ACQUISITION SYSTEM

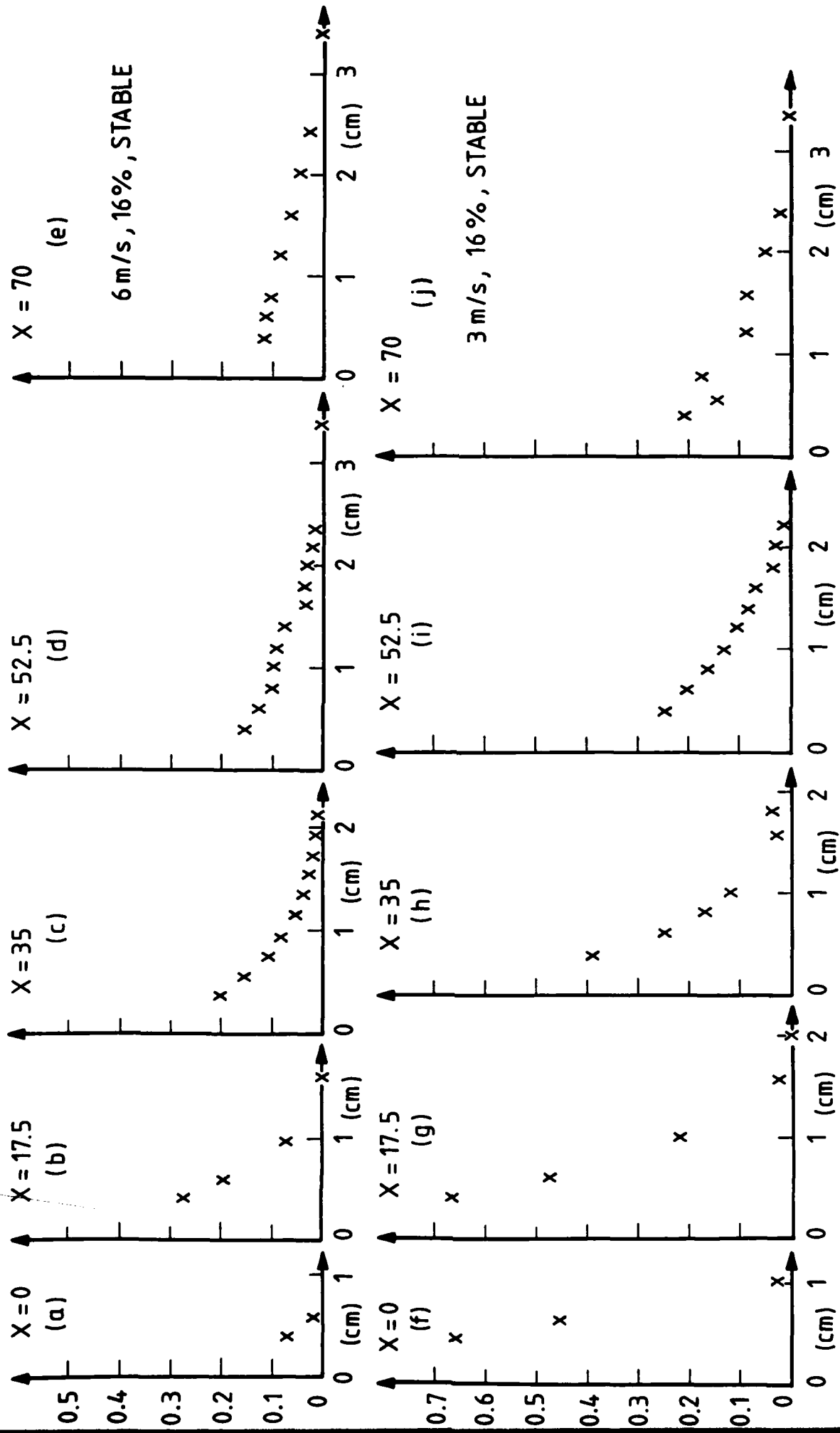


FIG. 3-4 - GAS CONCENTRATION MEASUREMENTS VS. HEIGHT FOR STABLE CASE



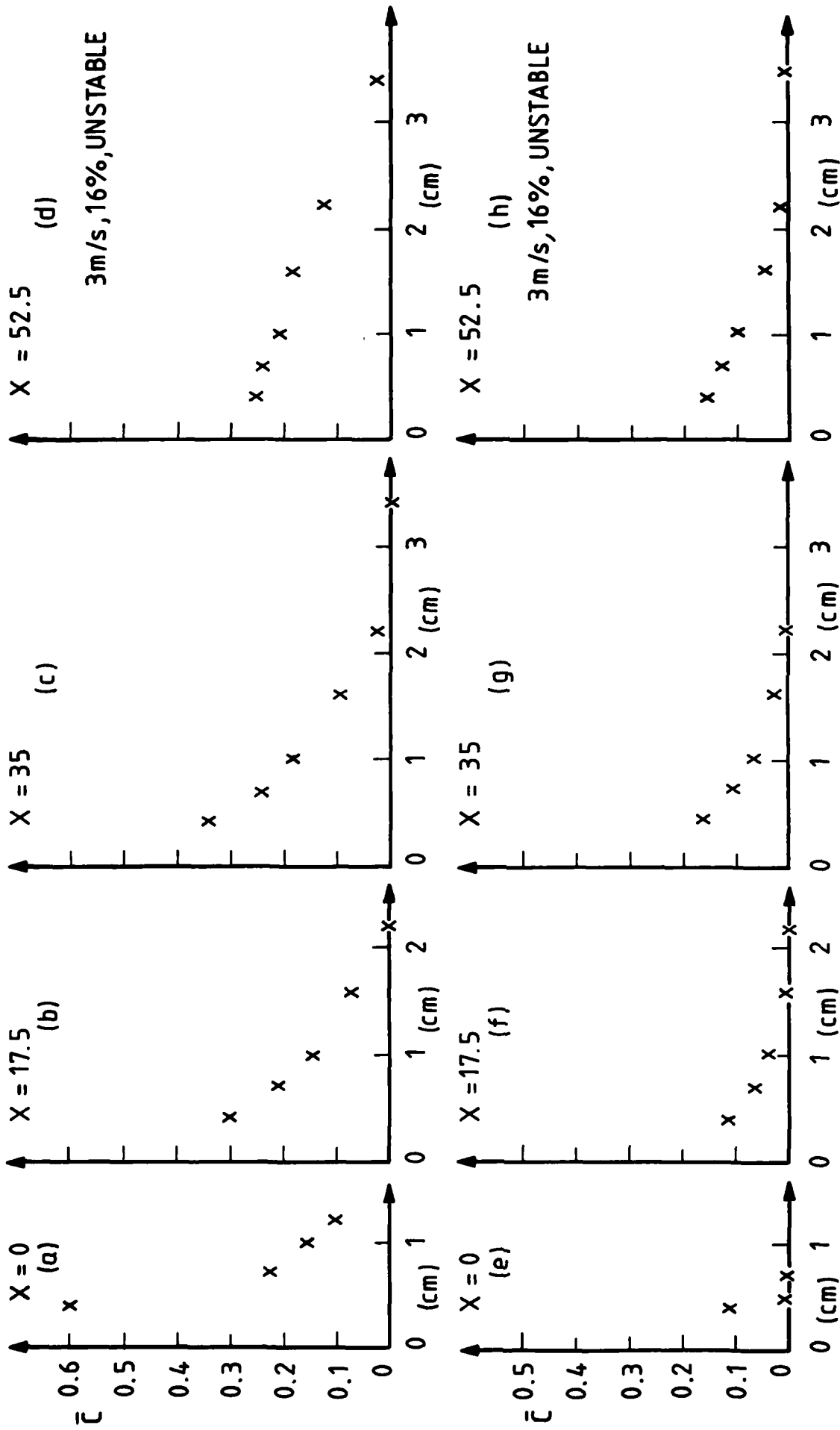


FIG. 3-5 - GAS CONCENTRATION MEASUREMENTS VS. HEIGHT FOR UNSTABLE CASE



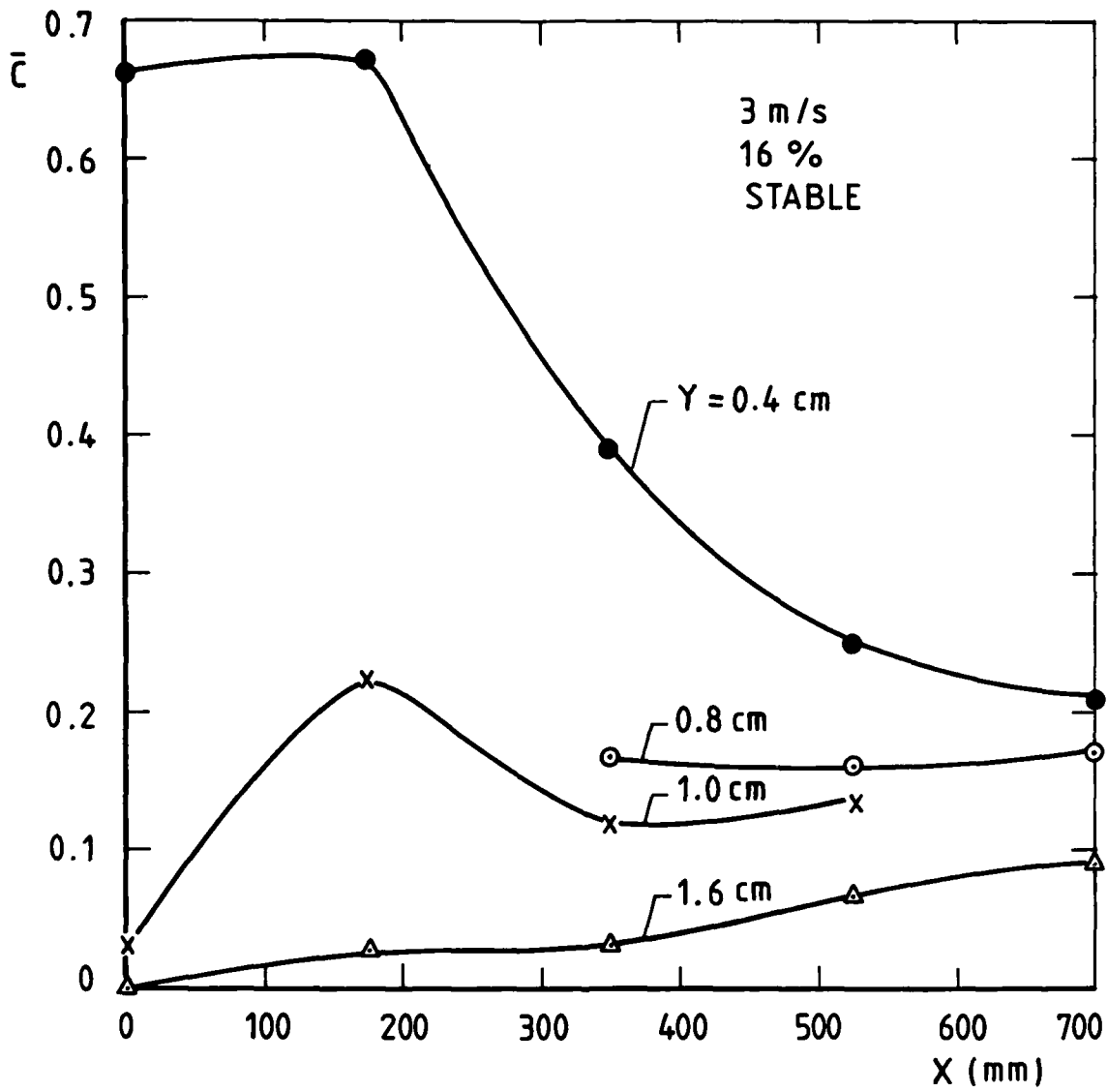


FIG. 3 - 6 - GAS CONCENTRATION MEASUREMENTS VS. DOWNSTREAM DISTANCE FOR STABLE CASE

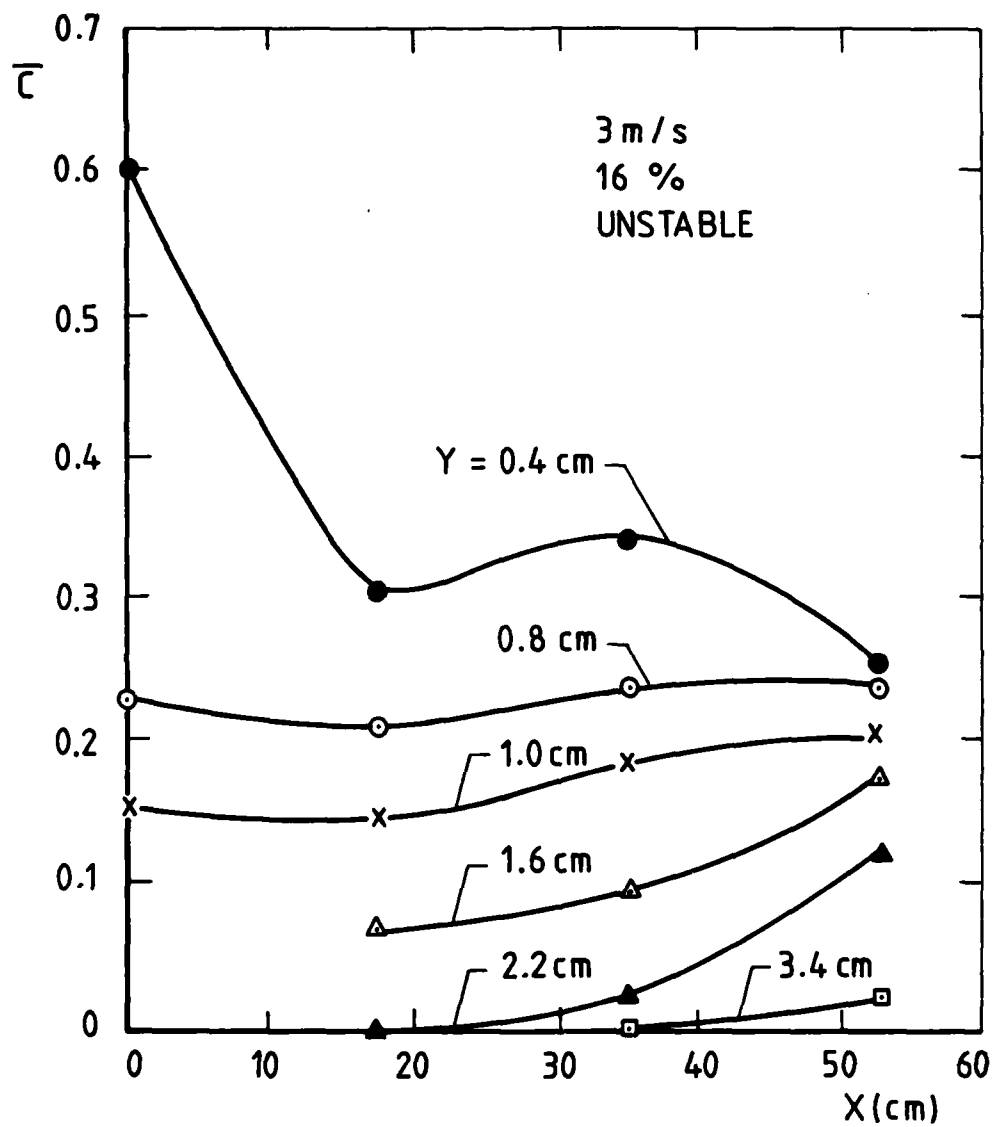


FIG. 3-7 - GAS CONCENTRATION MEASUREMENTS VS. DOWNSTREAM DISTANCE FOR UNSTABLE CASE

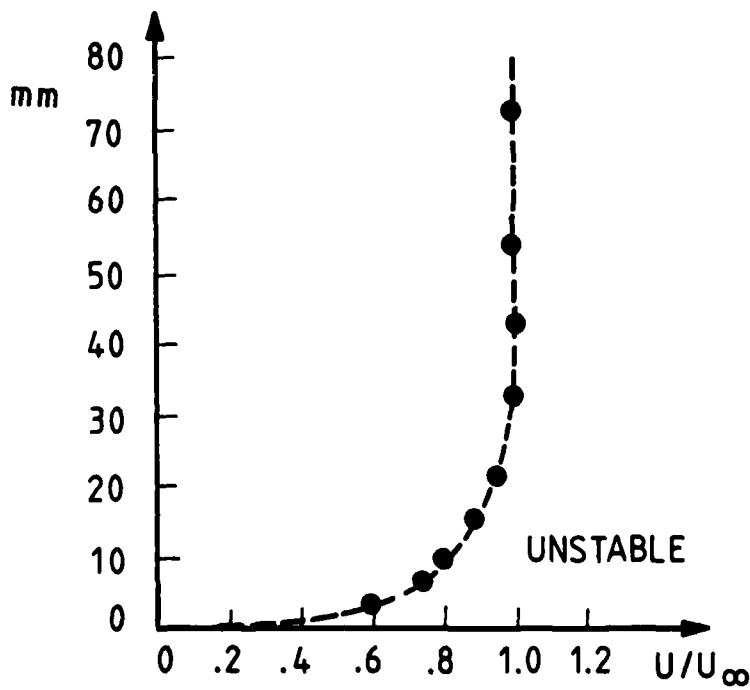
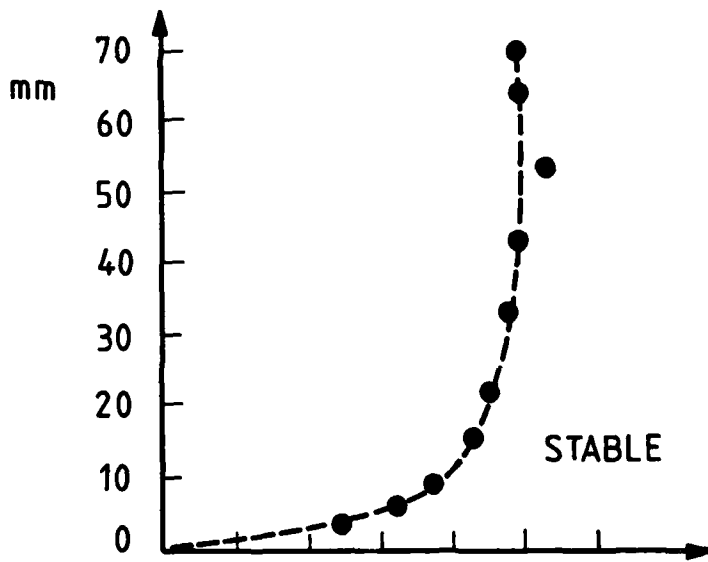
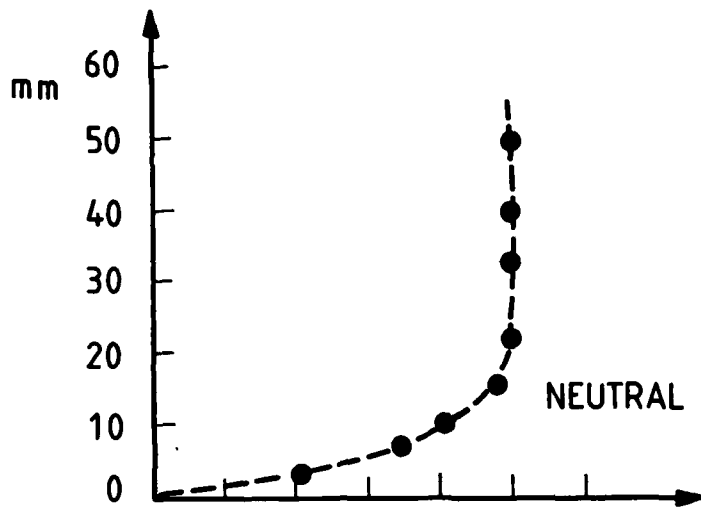


FIG. 3.8 - MEAN VELOCITY PROFILES $\frac{x}{a} = 1.5, U_{\infty} = 3 \text{ m/s}$



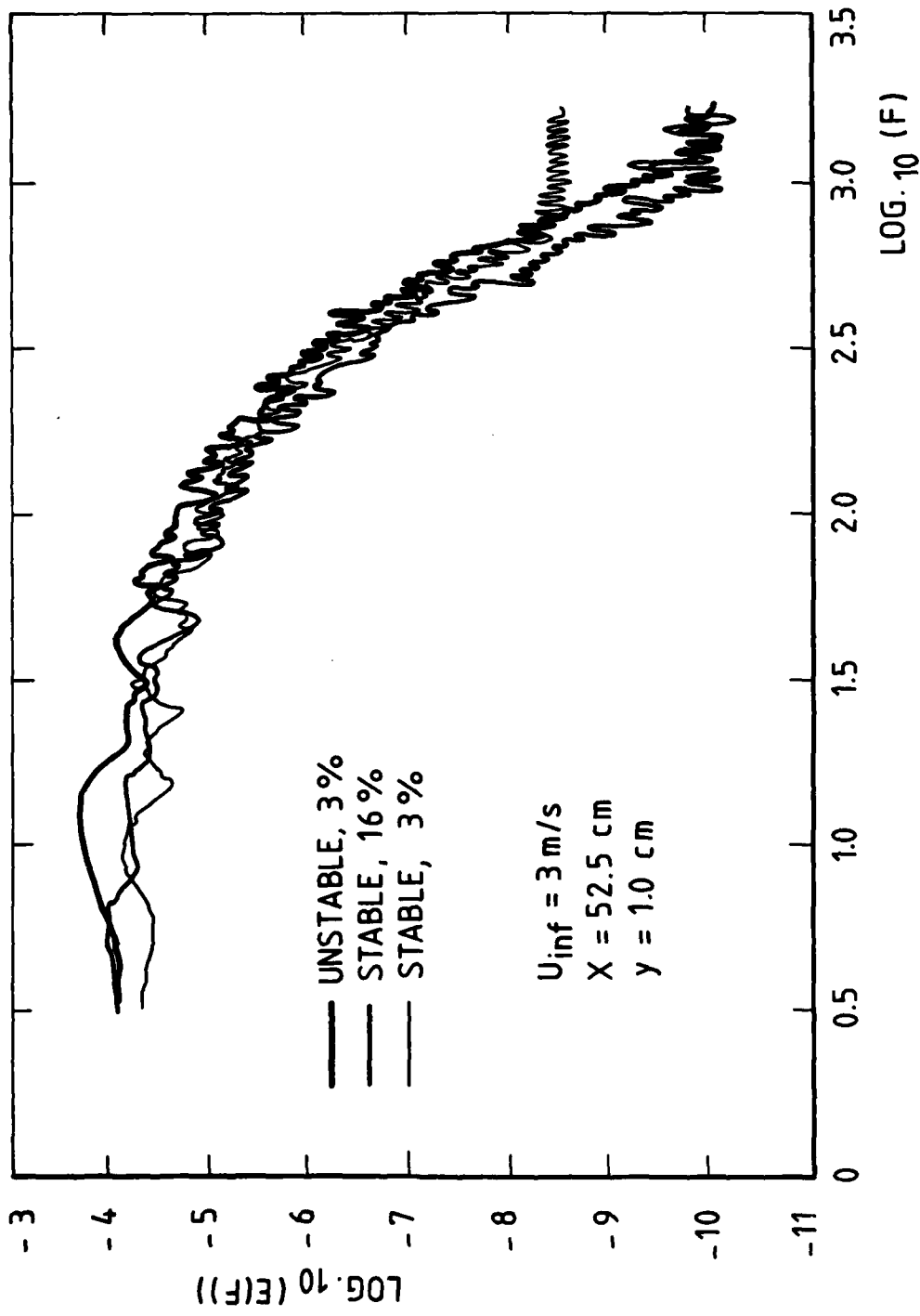


FIG. 3.9 - POWER SPECTRA OF CONCENTRATION



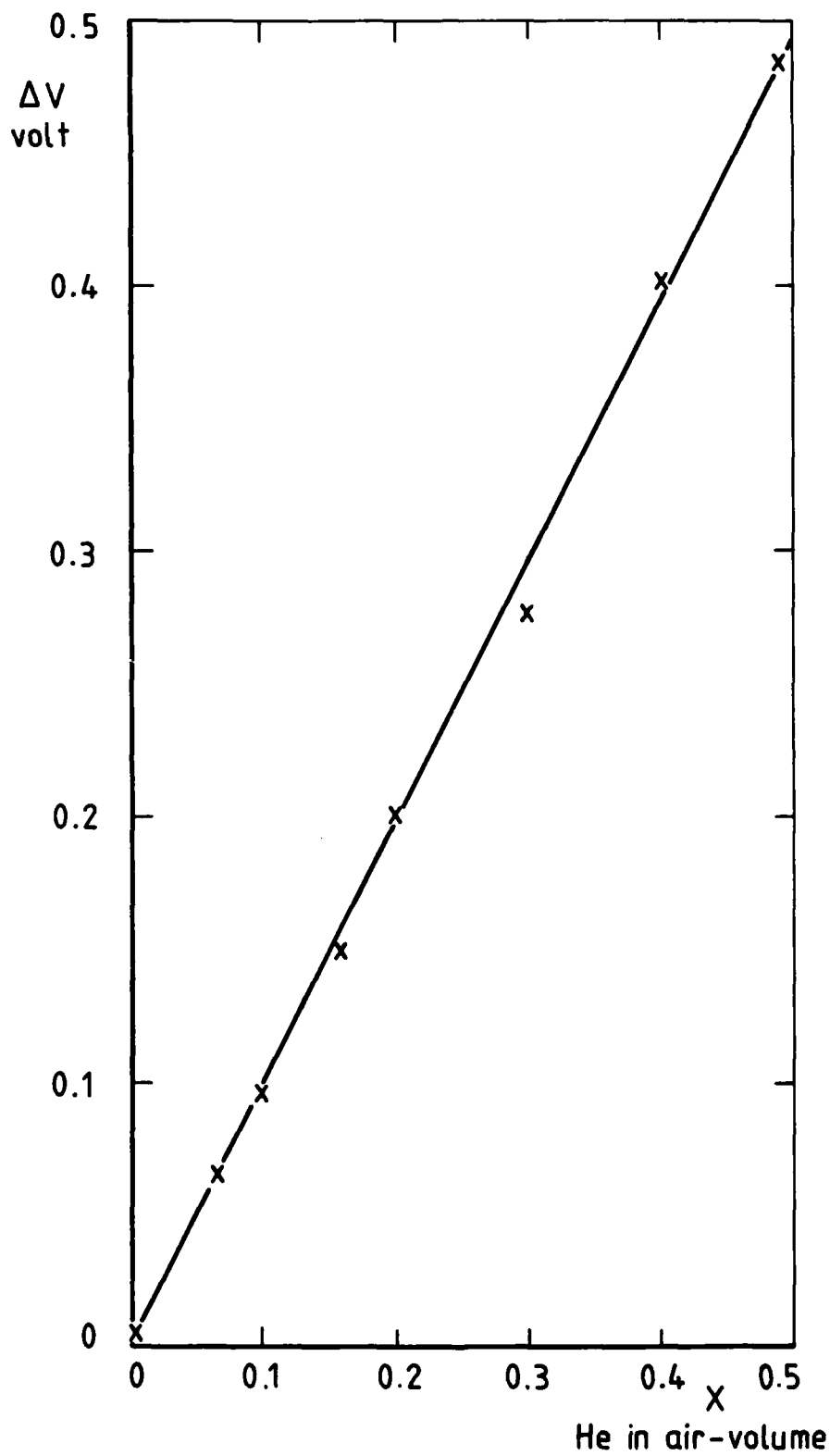


FIG. 3.10- EXAMPLE OF CALIBRATION CURVE OF THE MINIATURE CONCENTRATION PROBE

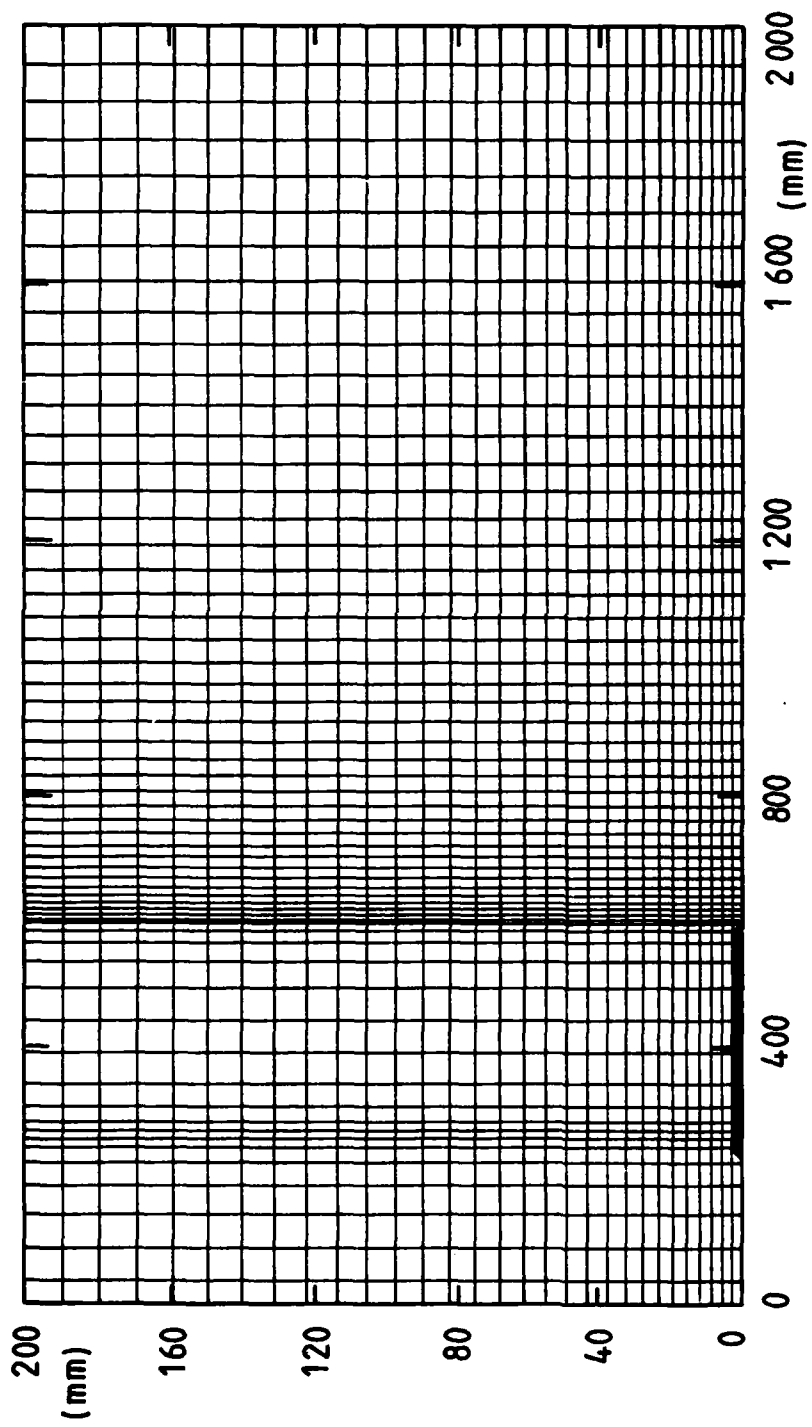


FIG. 4.1 - NXSTEP = 60 , XL = 2 000 , b = 300
ILLUSTRATIVE GRID A



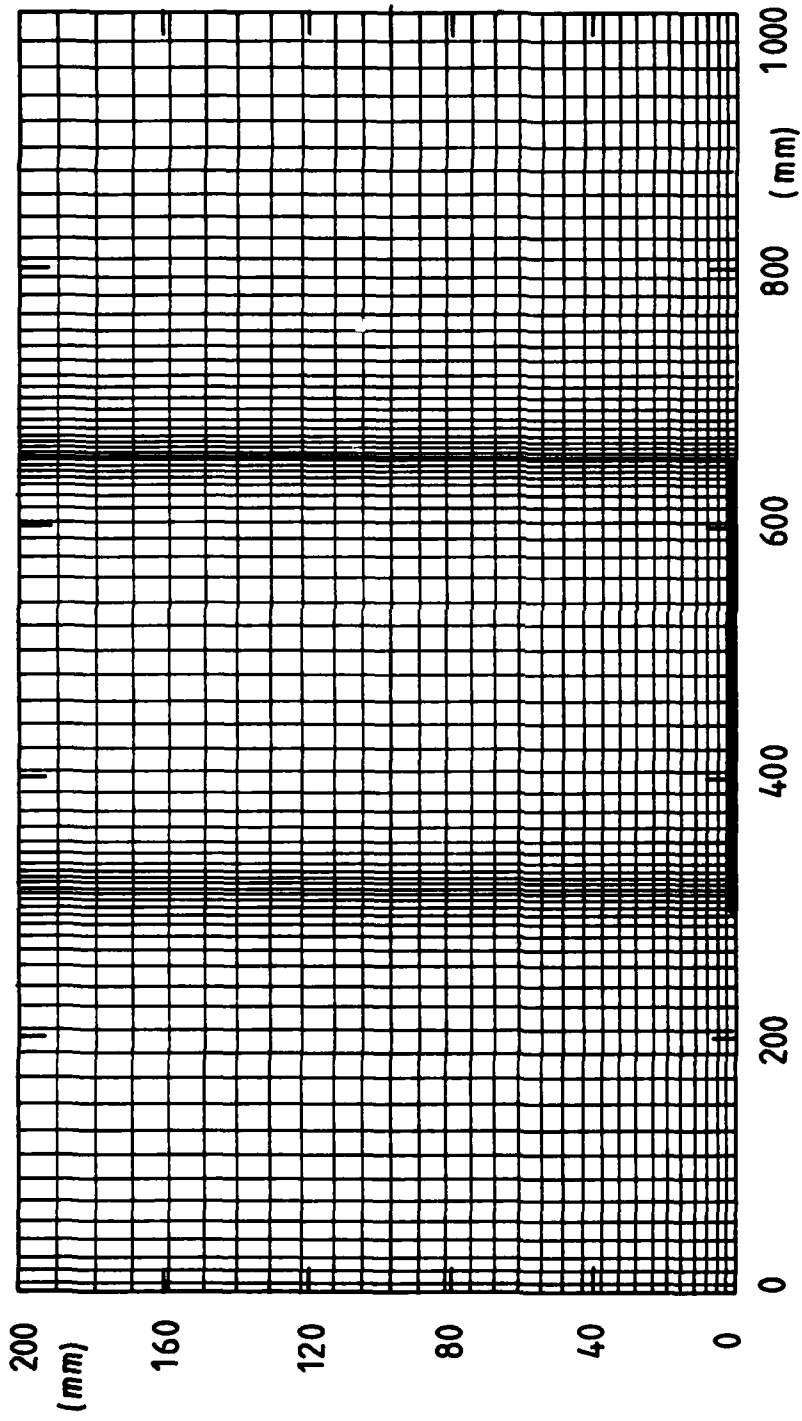


FIG. 4.2 - NXSTEP = 80 , XL = 1000 , b = 300
ILLUSTRATIVE GRID B



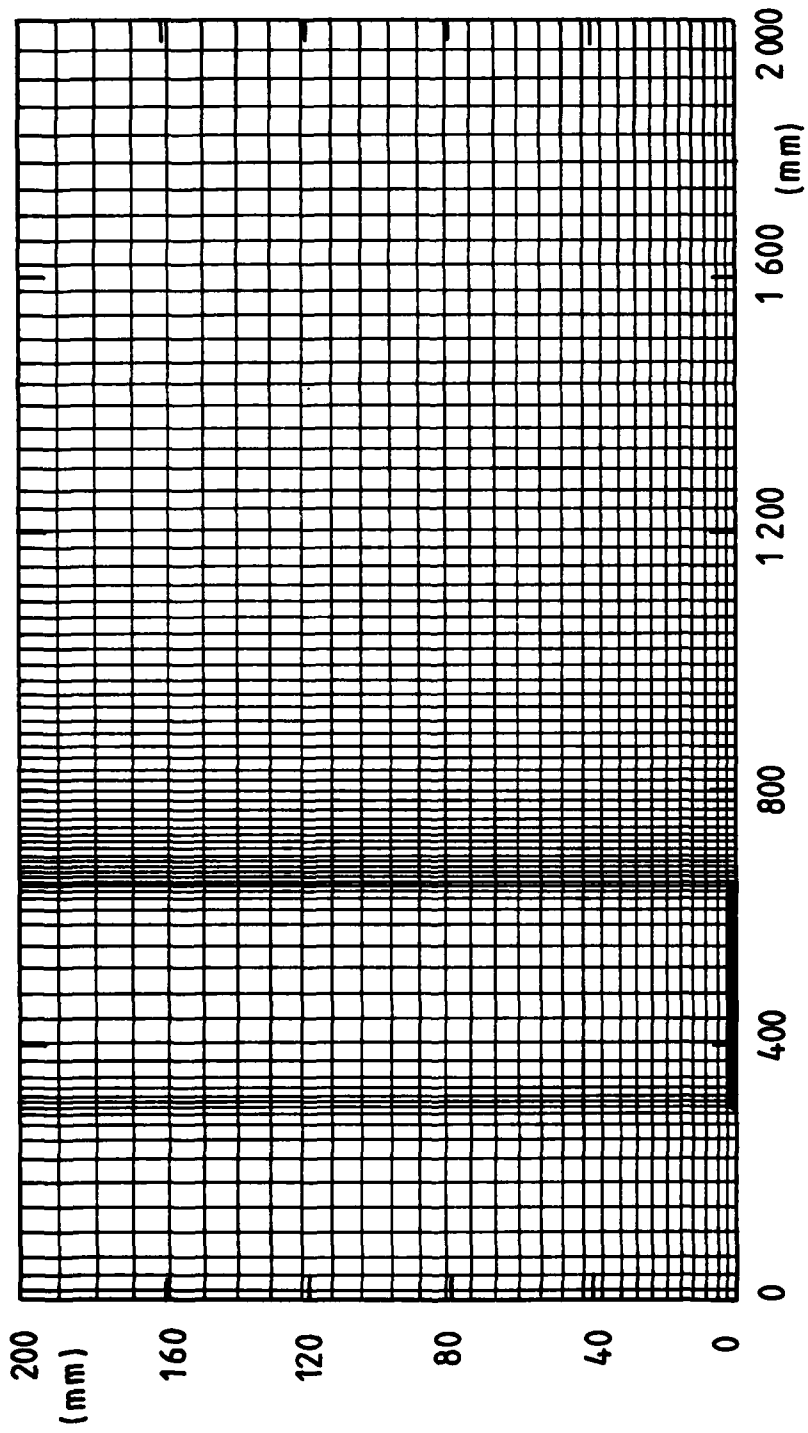
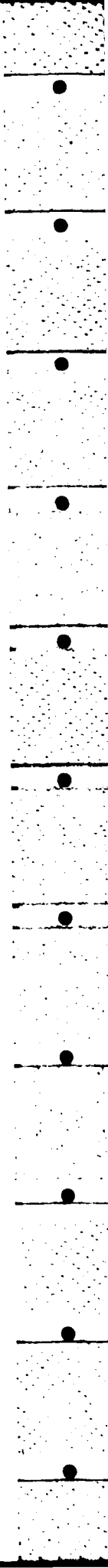


FIG. 4.3- XL = 2000 , b = 350 , NXSTEP = 80
ILLUSTRATIVE GRID C



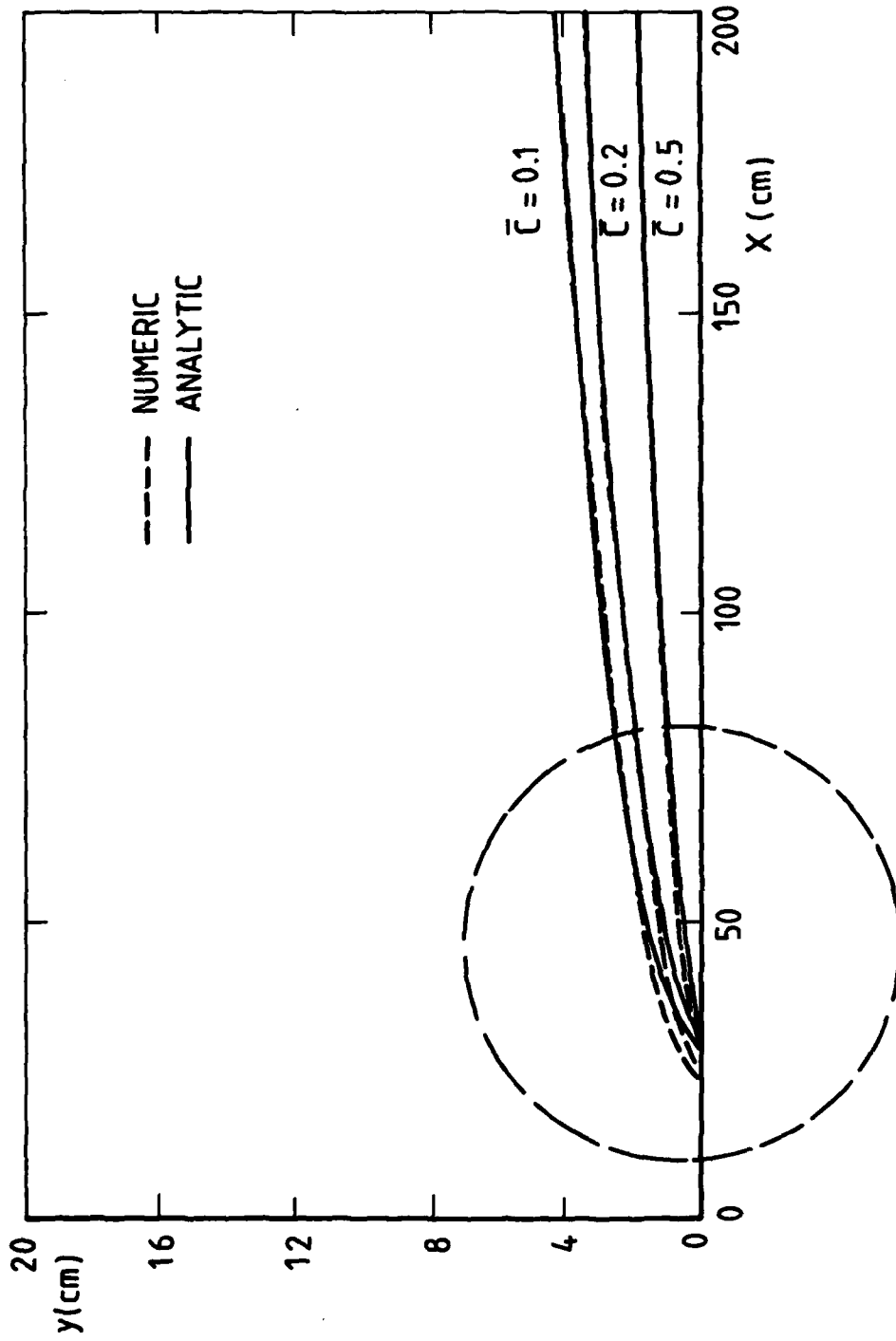
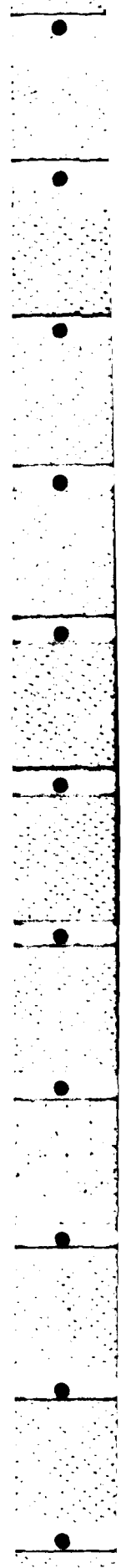


FIG. 4.4 - COMPARISON OF ISOCONCENTRATION CURVES



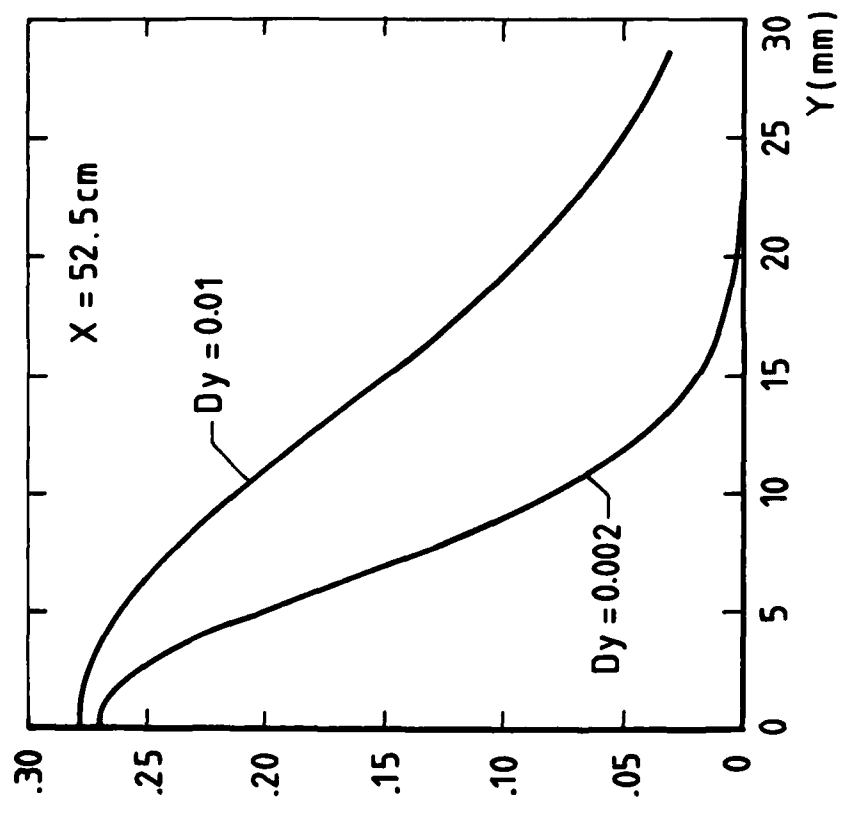
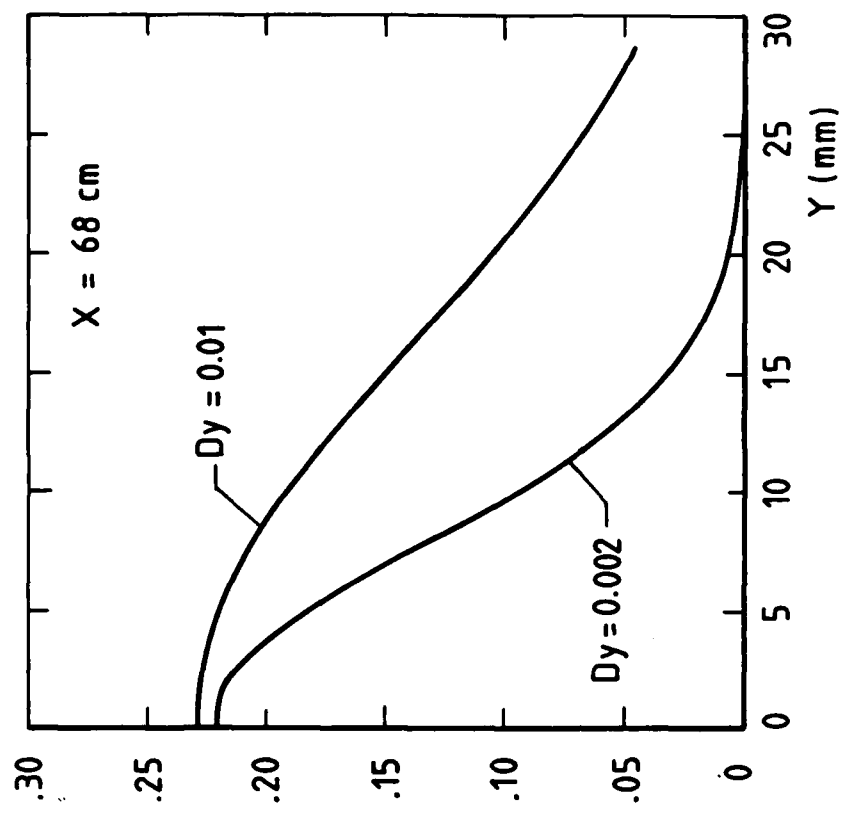
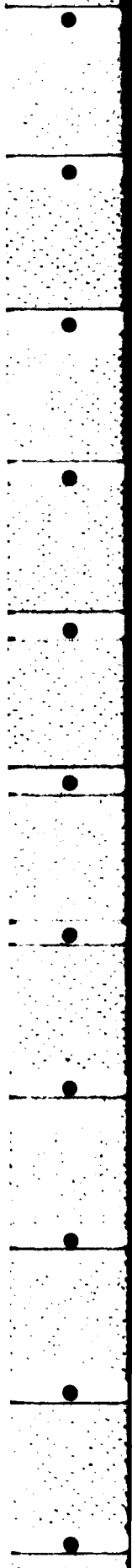


FIG. 4-5 - EFFECT ON GAS CONCENTRATION OF CHANGE IN Dy



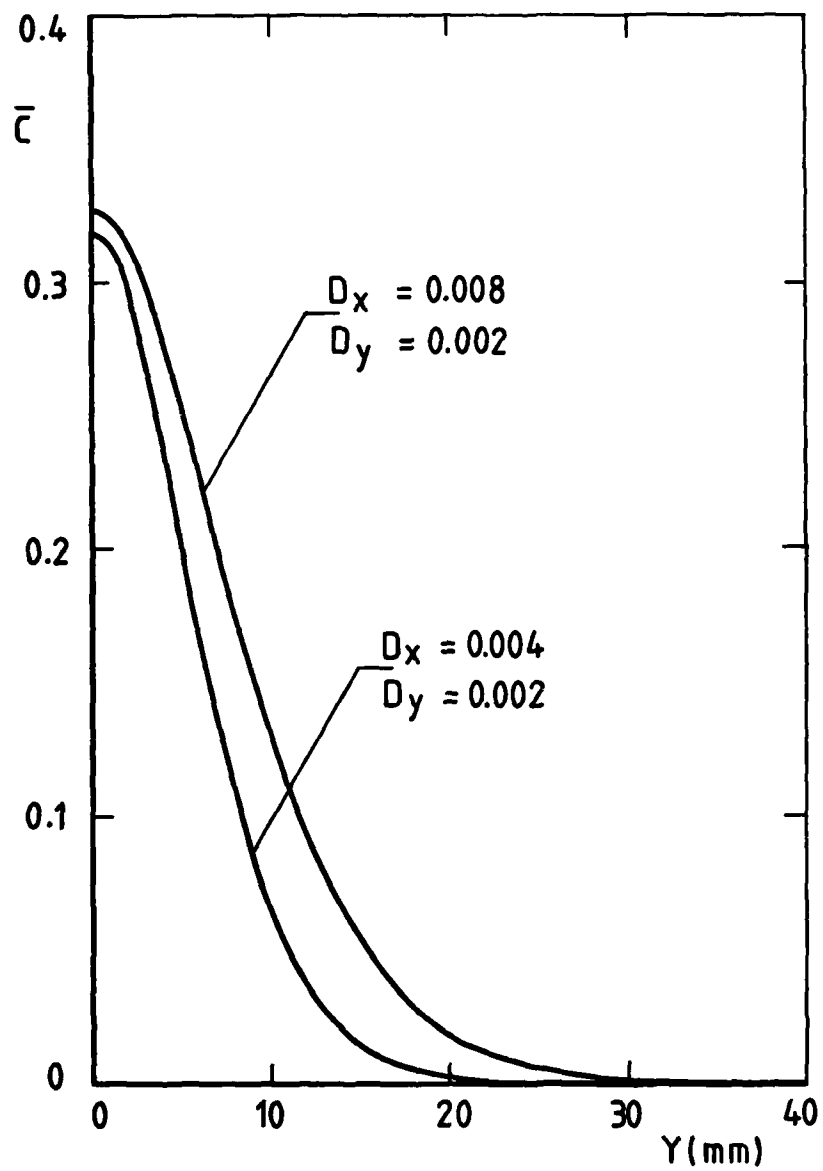
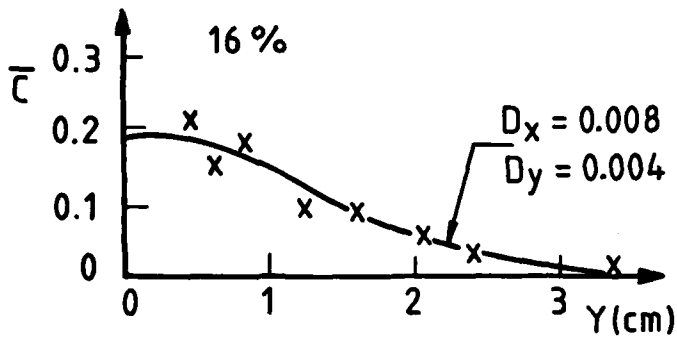


FIG. 4-6 - THE EFFECT ON CONCENTRATION OF A CHANGE IN U_{inf}



X = 70 cm
3 m/s, STABLE

$$D_x \propto \frac{u_{rms}}{U}$$

$$D_y \propto \frac{v_{rms}}{U}$$

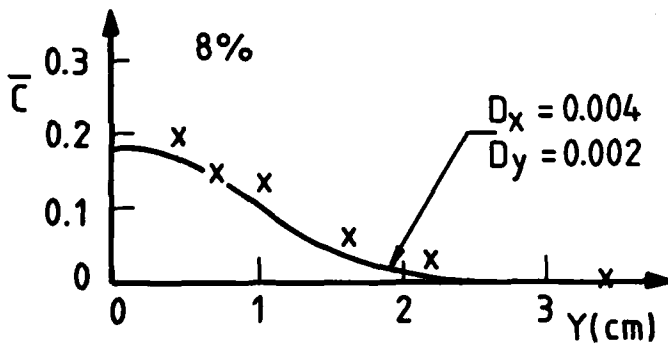
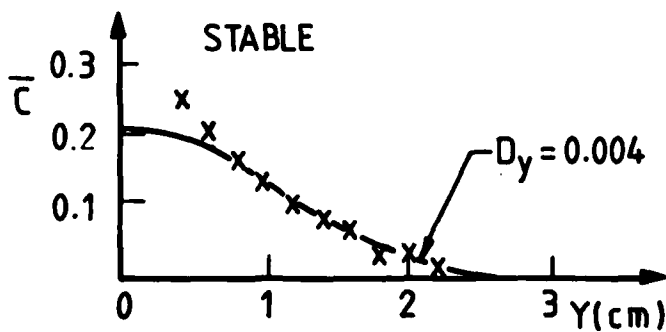


FIG. 4.7 (a) - EFFECT OF TURBULENT INTENSITY



X = 52.5 cm
3 m/s, 16%

$$\frac{D_{y, \text{heavy}}}{D_{y, \text{light}}} = 5$$

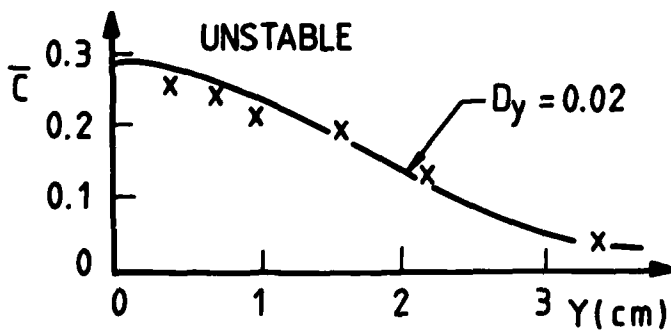
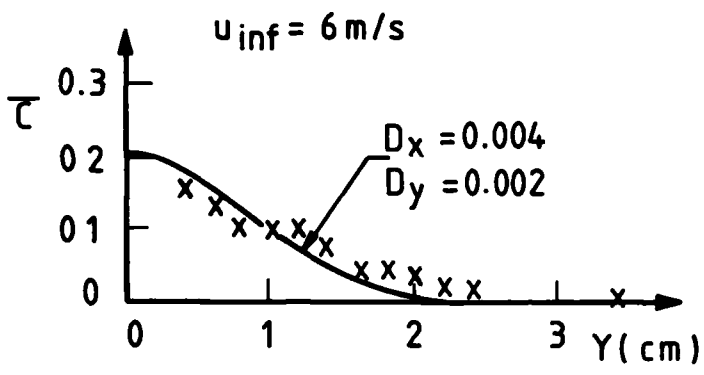


FIG. 4.7 (b) - GRAVITY EFFECTS



X = 52.5 cm
STABLE
16 %

$$D_x = \frac{D_{x \text{ phys}}}{U_{inf} L_x}$$

$$D_y = \frac{D_{y \text{ phys}}}{U_{inf} L_y}$$

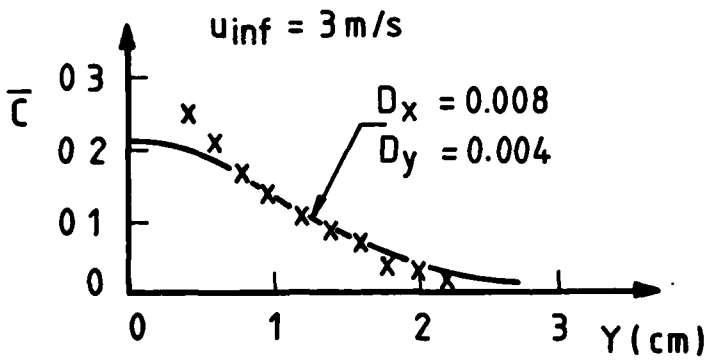


FIG. 4.8 - EFFECT OF CHANGING U_{inf}

END

FILMED

9-84

DTIC